San Jose State University
SJSU ScholarWorks

Master's Theses   Master's Theses and Graduate Research

2008

Sol-gel template-directed synthesis of oxide and carbide nanowires

Penny Lim Tan
San Jose State University

Follow this and additional works at: https://scholarworks.sjsu.edu/etd_theses

SOL-GEL TEMPLATE-DIRECTED SYNTHESIS OF OXIDE AND CARBIDE

NANOWIRES

A Thesis

Presented to

The Faculty of the Department of Chemical and Materials Engineering

San Jose State University

In Partial Fulfillment

of the Requirements for the Degree

Masters of Science

by

Penny Lim Tan

May 2008

UMI Number: 1458163

INFORMATION TO USERS

The quality of this reproduction is dependent upon the quality of the copy
submitted. Broken or indistinct print, colored or poor quality illustrations and
photographs, print bleed-through, substandard margins, and improper
alignment can adversely affect reproduction.

In the unlikely event that the author did not send a complete manuscript
and there are missing pages, these will be noted. Also, if unauthorized
copyright material had to be removed, a note will indicate the deletion.

UMI®
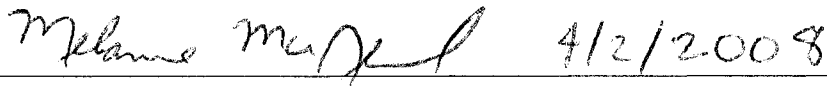
APPROVED FOR THE DEPARTMENT OF CHEMICAL AND MATERIALS
ENGINEERING

_____

Dr. Emily Allen

_____   4/2/2008
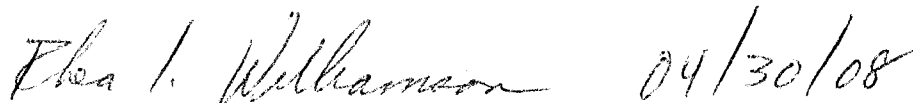
Dr. Melanie McNeil

_____

Dr. Geetha Dholakia, NASA Ames Research Center

APPROVED FOR THE UNIVERSITY

_____   04/30/08

ABSTRACT

SOL-GEL TEMPLATE-DIRECTED SYNTHESIS
OF OXIDE AND CARBIDE NANOWIRES

by Penny Lim Tan

Porous alumina templates were fabricated using cold temperature and room temperature anodization procedures. Template development at every stage of the room temperature procees was monitored. Alumina nanowires were found on the template surface after both the etching and the second anodization phases. Templates made using the room temperature procedure had pore diameters around 50 nm and interpore distances around 115 nm, wheras the and 0 °C anodized templates had similar pore features with pore diameters around 30 nm and interpore distances around 105 nm.

Nanowires of nickel oxide and iron oxide were successfully synthesized on commercial templates with 200 nm pore diameter Nickel oxide nanowires were also synthesized on fabricated templates with 50 nm pore diameter. Attempts were made to produce silicon carbide nanowires, however, the template method as well as procedures using temperatures cooler than literature values with longer annealing time periods were not successful.

ACKNOWLEDGMENTS

TABLE OF CONTENTS

LIST OF TABLES

LIST OF FIGURES

x

CHAPTER ONE

INTRODUCTION

1.1   The Development of Nanotechnology

Nanotechnology can be defined as the manipulation, customization and assembly

of materials from the atomic or molecular level to achieve specifically designed

attributes. This concept is not as new as it sounds. In fact, the late Nobel physics

laureate, Richard Feynman, in his 1959 talk *"There's Plenty of Room at the Bottom* [1],"

discussed the bottom-up as opposed to the top-down approach to designing and

synthesizing materials. The serious study of nanotechnology is more nascent, officially

beginning with the discovery in the 1980s of the buckminsterfullerene or "buckyballs," a

polymorph of carbon synthesized by Richard Smalley and Harry Kroto; and the

advancement in microscopy through the development of the Scanning Tunneling

Microscope (STM) by Gern Binnig and Heinrich Rohrer [2]. The discovery of

buckyballs was followed with the discovery of carbon nanotubes, the cylindrical

allotropes of these buckyballs [3]. Due to their size and structure, carbon nanotubes

exhibit unique electrical properties and are incredibly strong. Yu *et al.* [4] measured the

tensile strength of a set of 19 multiwalled carbon nanotubes and obtained values that

range from 11 to 63 GPa. Since the discovery of carbon nanotubes, other nanostructured

organic and inorganic materials such as nanoribbons, quantum dots, and nanowires have

been made.

1.2 Significance and Application of Nanowires

Nanowires are materials that have radii in the nanometer range and lengths from several microns to tens of microns; they are classified as pseudo-one dimensional materials. At small enough diameters, these materials may start to exhibit quantum effects such as electron confinement. The small size leads to electronic and magnetic properties that may deviate from that observed in the bulk phase [5].

Nanowires may play a key role in the miniaturization of devices. Already, simple electrical components such as transistors [6], p-n junctions [7] and logic gates [8] are being fabricated using nanowires. Aside from miniaturization, fundamental material properties can be investigated in nanowires whose diameters are small enough such that quantum effects start to produce properties that deviate from bulk behavior. For example, it is predicted that at diameters below 8 nm, the Morin temperature of hematite (α-Fe_2O_3) nanoparticles disappears [9]. Studying and developing an understanding of the effects of nanowire size vs. the resulting physical property may lead to the development of new or better uses for these materials. Another important feature of nanowires are their large surface areas ensuing from their large aspect ratios. This property makes this type of material attractive for sensors and detectors. An exciting study by researchers G.F. Zheng *et al.* [10] reported the use of silicon nanowires in detecting certain cancer biomarkers in blood samples. The research and development of nanowires is only a few decades old, however, it is a promising field already being studied for its potential as the next generation of electronic components, sensors [11] and composites [12].

1.3 Synthesis of Nanowires

This section presents the various methods by which nanowires are synthesized. Section 1.3.1 presents an overview of the most common nanowire synthesis methods including both templated and non-templated processes. Section 1.3.2 goes into more detail on template-directed sol-gel nanowire synthesis.

1.3.1 Overview of Nanowire Synthesis

Nanowires have been synthesized largely by the chemical vapor deposition method (CVD). The principle of CVD for nanowire growth is to first seed catalysts onto a substrate; these catalysts serve as nucleation sites for nanowire growth [13]. Feed gas containing the chemical precursors are then introduced to the substrate which react at the catalyst site. Nanowire growth mechanisms include Vapor-Liquid-Solid (VLS) and Vapor-Solid (VS) mechanisms. CVD's popularity stems from the excellent purity of the resulting product as well as the procedural simplicity, however, a number of factors do affect the characteristics of the resulting nanowire and require fine tuning. These factors include pressure, temperature, catalyst type, reactor geometry, etc. Also, the scope of materials applicable to this process is limited by the precursor availability in the gaseous form. Silicon [14], gallium nitride [15] and tin oxide [16] are some examples of nanowires that have been produced using CVD.

The use of molds or templates to create nanowires is also popular. Control of nanowire morphology has been attempted in many types of templates ranging from

3

porous alumina to micelles [17]. Templates, particularly polycarbonate and alumina templates, are commonly used in electrodeposition. Electrodeposition involves using a template with conducting material attached on one end to use as an electrode, while the solution containing reagent electrolytes is placed in between the template and a counter electrode. Voltage is applied and the pores are filled electrochemically. Gold [18], cobalt [19] and nickel [20] are some examples of nanowires that have been produced via electrochemical deposition. A similar procedure known as electrophoretic deposition also uses templates to create nanowires. The difference between electrophoretic and electrochemical deposition is that for electrophoretic deposition, instead of reagent electrolytes that react into the desired material, colloidal suspensions of that material are already made and voltage is supplied only to induce the migration of these colloids into the pores. An annealing step may be applied if necessary to fuse and crystallize the nanowires. Examples of materials made into nanowires through electrophoretic deposition are tellurium [21], hematite [22] and zinc oxide [23].

A number of solution methods to synthesize nanowires have also been explored such as hydrothermal reactions [24] as well as other in-solution methods [25-26], where colloidal growth of the nanomaterial is controlled with or without capping agents.

Sol-gel chemistry is a wet chemical method that is being utilized to create nanowires [27-28]. The attractive features of using the sol-gel method are its economy, relative simplicity and scalability. The method also lends itself to the use of templates to mold the nanowire into its desired shape and size. The sol-gel method is a flexible

method which has long been used to make a variety of materials including complex oxides, sulfides and nitrides.

1.3.2 Synthesis of Nanowires by Sol-Gel Method

The sol-gel process entails a phase transition from one colloidal phase to another. A colloidal system is a mixture where the dispersed phase has a large surface to volume ratio. These systems would thermodynamically prefer to aggregate, but do not because surface chemistry slows down this process [29]. Sols are colloids in which the continuous phase is a liquid and the dispersed phase is a solid. Paint is an example of a sol. Gels are the opposites of sols; the continuous phase is a solid and the dispersed phase is a liquid. Hair gel is an example of a gel. In sol-gel chemistry, sol precursors form in the liquid medium, and then a polymerization reaction occurs where sol precursors grow, link and eventually span into a continuous network, forming a gel. The two main reactions are usually a hydrolysis reaction and a condensation reaction [30].

To make nanowires using the sol-gel method, it is sometimes possible to use a template with pores of defined length and diameter. The sol must be able to permeate the pores of the template for this method to work. There is also the question of separating the nanowires from the template. To use the template the usual procedure requires that the sol be formed, the template is then dipped into the sol for a prescribed amount of time and then dried to form a gel inside the pores. For simple oxide compounds, only an annealing process is usually required to finish the process - solidifying the nanowire and

adjusting it to the desired crystalline phase. For non-oxide compounds such as carbides

and nitrides, the synthesis is more complex. The resulting gel may have extraneous

elements and/or may not contain all the necessary elements to form the desired

compound, requiring a hybrid method where a gel is still formed but an additional

chemical reaction with the gel is performed, in conjunction with or followed by an

annealing step.

1.4   Porous Alumina Templates

Nanoporous templates have played a large part in nanowire synthesis and a

variety of materials to provide these templates including polymer [31], glass [32], mica

[33] and anodic aluminum oxide [23] have been investigated. Among these templates,

anodic aluminum oxide templates have gained the most popularity not only because of

the ease of synthesis, but also the ability to control the pore size and the pore length with

simple adjustments to the anodizing conditions. Also, unlike templates fabricated using

nuclear track-etched methods such as the polymer and mica templates, anodized alumina

pores are parallel to one another. At temperatures up to 700 $^{\circ}$C, anodized alumina

templates are composed largely of hydrated alumina and Υ-alumina and may be dissolved

with acid or base solutions. However, above 700 $^{\circ}$C, the alumina template will start to

crystallize, moving through different phases until 1000 $^{\circ}$C and above, where the

thermodynamically stable and chemically resistant alpha phase forms [34]. The

temperature range prior to the phase transformation of the alumina templates

accommodates a wide number of sol-gel derived ceramic materials whose annealing

temperature falls within this range, allowing the release of nanowires by simple dissolution of the template.

In this thesis, nickel (II) oxide (NiO), hematite (α-Fe$_2$O$_3$) and silicon carbide (SiC) nanowires were grown using the sol-gel technique and characterized using methods which are described in chapter three. The properties of these compounds are briefly detailed below.

NiO is a wide band-gap semiconductor and is antiferromagnetic. It has been used in gas sensors, fuel cells and electrochromic devices [28, 35-36].

In its bulk phase, α-Fe$_2$O$_3$ is weakly ferromagnetic, but as nanomaterials, the magnetic properties are known to vary as a function of size [9]. Suber *et al.* [37] note that magnetic nanowires exhibit perpendicular anisotropy and would allow higher recording capacities for disk heads. Hematite nanostructures are also being explored in gas sensing and lithium ion battery applications [38].

Silicon carbide is a wide band-gap semiconductor with high thermal conductivity and can be used for high temperature and high power applications. Its hardness is close to diamond and may be useful for composites [39].

1.5   Characterization of Nanowires

Complete characterization of nanowires involves a number of measurements. For the most part, a successfully prepared nanowire is of the desired dimensions and chemical composition, non-hollow and may have a single crystal or polycrystalline structure. To

determine how successfully the nanowires were synthesized, a Scanning Electron

Microscope (SEM) is first used to provide visual confirmation of the morphology. Next,

to determine if the correct compound formed, Energy Dispersive X-Ray Spectroscopy

(EDS) is used to provide elemental analysis. Finally, to determine the structure of the

nanowires, Transmission Electron Microscopy (TEM) or X-Ray Diffraction (XRD) are

commonly used.

CHAPTER TWO

LITERATURE REVIEW

2.1   Literature Review

In this chapter, the pertinent literature relating to the sol-gel synthesis of oxide

and carbides nanowires, as well as literature on the fabrication of aluminum oxide

templates will be discussed. Section 2.2 will present a short background as well as the

growth theories of porous anodic alumina and the variables that control the pore

structure. Section 2.3 discusses the use of templates to grow nanostructured materials

and their role in the synthesis of oxide nanowires. Section 2.4 discusses the sol-gel

synthesis of bulk carbides and the various materials that have been investigated for the

carbon source. Finally, Section 2.5 examines the current state of research in growing

carbide nanowires - specifically, silicon carbide nanowires. Finally, Section 2.6 provides

a chapter summary.

2.2   Growth and Feature Control of Porous Anodic Alumina

Anodized alumina has been used since the early 1900s, especially for its corrosion

protection and its insulating properties. It was observed however, that porous alumina

could be formed under the right anodizing conditions. The examination of the self-

assembly of nanoholes on anodized alumina began in the 1950's. In a study reported in

1978 by Thompson *et al*. [40] using phosphoric acid as the electrolyte and a current

density of 50 A/m^2, researchers showed cross-sectional TEM micrographs of the metal/ film regions of aluminum anodized for 20, 120 and 160 seconds which showed the scalloping and eventual pore formation on the surface. They theorized that the oxide layer between the metal and electrolyte forms faster around defect sites, either grain boundaries or on ridges, while the areas surrounding the defect start to develop a scalloped texture. As anodization continues, due to electric field variations in the ridged and scalloped areas, pores develop at sites which had larger scalloped regions because the rate of film formation is enhanced at the ridges and depressed at the scalloped areas.

The pores consisted of two layers: a pure alumina layer caused by direct oxidation of Al^{3+}, by the ingress of OH$^-$ and O^{2-} ions from the electrolyte, and an impure hydrous alumina layer consisting of ejected, unconsumed Al^{3+} which is then deprotonated and formed into colloidal hydrous alumina. The colloids aggregate and are then deposited onto the film-solution interface including with it some of the electrolyte anions. Figure 1 illustrates the pore structure as well as the ion migration behavior during anodization. At steady-state, direct oxidation as well as hydrous alumina deposition are in equilibrium with the field-assisted dissolution of the alumina film, which keeps the barrier layer thickness as well as the pore diameter constant even as the pores continue to grow in length.

In 1981, Thompson and Wood [41] studied the effect of the anodizing electrolyte on the steady-state growth behavior of porous alumina at 20 V. Anodization times were not reported. The authors report that the ratio between the thickness of the pure inner
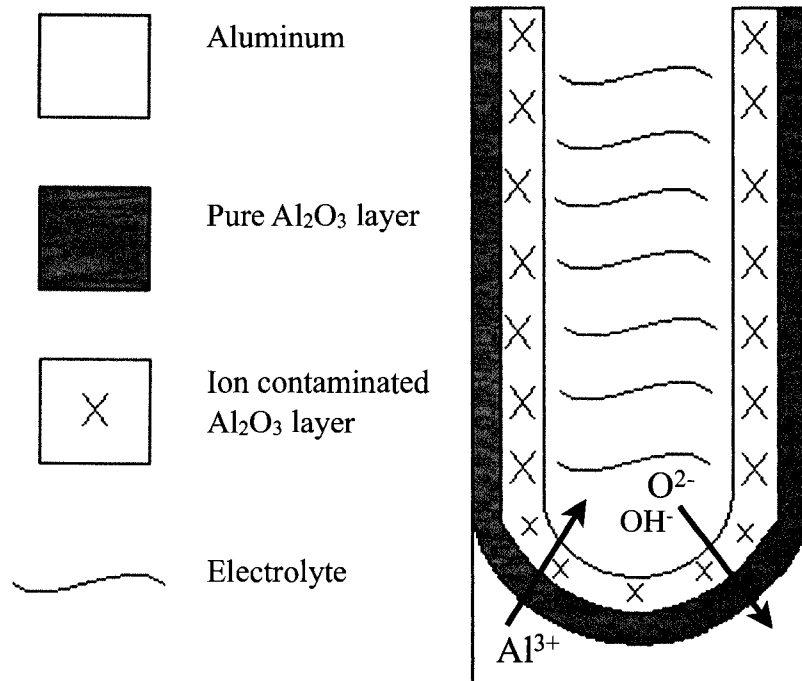
Figure 1. An illustration of an alumina pore grown from an anodization procedure.

alumina layer and the thickness of the impure outer layer strongly depends on the electrolyte type, with sufuric acid, oxalic acid, phosphoric acid and chromic acid giving an inner layer to outer layer thickness ratio of 0.05, 0.1, 0.5 and infinity, respectively. The authors argue that the ion migration through pure alumina is the rate determining step for the ion-contaminated alumina layer formation and that the larger the true field across the alumina, the faster the growth of this layer. Hence, sulfuric acid grown alumina, which has a larger true field across the pure alumina region with an inner/outer

layer thickness ratio of 0.05 will have a faster rate of film formation than that of phosphoric acid grown alumina which has a thickness ratio of 0.5.

The studies mentioned until now however, were performed on disordered porous alumina. It was not until 1995, in the process of fabricating platinum and gold nanohole arrays, that Masuda and Fukuda [42] developed and reported the first two-stage anodization method for fabricating porous alumina which produced templates with uniform, hexagonally packed nanohole arrays with long-range order.

Investigating the self-ordering mechanisms involved with forming ordered porous alumina, Jessensky et al. [43] proposed that due to the volume expansion of aluminum to alumina during the oxidation process, mechanical stress develops at the metal-oxide interface and causes a repulsive force between neighboring pores, giving rise to the honeycomb structure. Nielsch et al. [44] claimed from TEM observations of well ordered porous alumna regimes made from suluric, phosphoric and oxalic acid, that ordered porous alumina has a constant ratio of pore radius and interpore distance regardless of how it was fabricated, and that from the equation:

$$P = (2\pi/\sqrt{3})(r/D_{int})^2 \qquad \text{Equation 1}$$

where P is the porosity, r is the pore radius and D_{int} is the interpore distance, the porosity of these well ordered regimes must be around 10%. Also, given

$$D_{int} = kU, \qquad \text{Equation 2}$$

where k is a constant relating pore interval to potential approximating 2.5 nm/V and U is the anodizing potential, an optimal U can be calculated for a given r and a porosity of 10% using the equation:

$$U = \sqrt{((2\pi)/(\sqrt{3}P))}(r/k).$$
Equation 3

Finally, Nielsch *et al.* [44] also claimed that anodization time affects the domain size in two ways. In the beginning stages of anodization, ordered domain sizes become larger as time increases. However, after some time passes, the trend reverses and ordered domain sizes decrease with time. This observation is in contrast to Li *et al.*'s [45] claim that domain size increases linearly with time.

Masuda and Fukuda's [42] two-stage anodization consists of three phases: the first is a long anodization, followed by etching of the alumina produced by the first anodization, and then a second anodization. The initial stages of the first anodization produces porous alumina with poor ordering. As anodization proceeds, the regularity at the pore bottom improves. The alumina layer is stripped off, leaving the pore pattern imprinted onto the aluminum surface. Re-anodization of this aluminum yields porous alumina with uniform pores and excellent long-range order. The alumina prepared by this method usually yields mostly amorphous alumina with some γ-phase alumina [46], as long as the process conditions do not provide enough heat to further its crystallization. The development of this two-stage anodization method led to the widespread use of porous alumina membranes as a template for nanostructured materials. Efforts from a variety of researchers have produced porous alumina with pore diameters between 5 and 150 nm [47-48] and interpore distances between 45 and 980 nm [49-50] using the

13

common anodizing electrolytes sulfuric, oxalic and phosphoric acid, as well as other organic acids [†]. Control of pore features is determined from the combination of anodizing voltage, electrolyte solution type and concentration. Other research on porous alumina includes the use of the additive sulfonic dye light green [51] to influence growth rate and pore features. In an effort to simplify the anodization process, a one step high field anodization using aged electrolyte solutions was also investigated [52].

Free-standing alumina membranes can be made by implementing additional steps to remove the barrier layer. The solution side of the template is covered with a protective layer. Nail polish has worked surprisingly well for this purpose [53]. The aluminum backing is removed using mercury chloride or copper chloride solutions [53]. The membrane is then dipped into a phosphoric acid solution to open the barrier layer. Recently, more simple methods for removing the barrier layer have been reported and employ a brief anodization pulse using a 1:1 mixture of 78% perchloric acid and 98% butanedione [54] or a 1:1 ethanol and 78% perchloric acid [55] solution at 10 V higher than the anodizing voltage.

2.3   Template Directed Sol-Gel Synthesis of Oxide Nanowires

Templated synthesis of nanostructured materials became increasingly popular in the early 1990s. In 1994, C.R. Martin [56] reviewed the preparation of nanomaterials using membrane-based synthesis, which included metals, polymers and semiconductors. As commercial membranes in a variety of pore sizes are available, templated synthesis

---

[†] Pore diameters are derived from anodization only. Larger pores can be obtained through pore widening procedures.

14

continues to be an attractive method due to its ability to control the dimensions of the materials made. Templated synthesis encompasses a variety of methods including electrodeposition, electropolymerization, solution methods or a combination of the above. Sol-gel templated synthesis of nanowires, however, came into being in the late 1990s. Schlottig *et al.* [57] were among the first to report sol-gel templated synthesis of nanowires. Template directed sol-gel synthesis of nanowires is widely used when oxide nanowires are made. Sol-gel chemistry had already been well developed, and the commonly used metal alkoxides, which readily react with water to form the metal-oxygen bonds, are cheap and abundant. The most common template used is the anodic alumina template (AAT). Various oxide nanowires have been made including insulators (TiO_2), semiconductors (SnO_2 and NiO) and ferromagnets (α-Fe_2O_3). In a typical experiment, the sol is synthesized, and at a viscosity where some gelation has occurred but the starting material is still able to infiltrate the pores, the template is dipped into the mixture for a prescribed amount of time and then annealed. After the heating process, the nanowires are released by dissolving the template in sodium hydroxide.

2.3.1 NiO Nanowire Synthesis

Table 1 shows the synthesis conditions used by various researchers to make NiO nanowires. Table 2 shows the results of the synthesis methods.

Table 1. NiO Nanowire Synthesis Parameters.

Research Group	Materials	Template (Pore Size)	Heating Conditions
Yang et al. (2005)	Nickel nitrate hexahydrate and citric acid	None	750 °C 8 hours
Yu et al. (2006)	Nickel nitrate hexahydrate and citric acid	AAT (30-60 nm)	500 °C 1 hour
Cao et al. (2006)	Nickel nitrate hexahydrate and hydrazine	AAT (100 nm)	600 °C 5 hours Argon

Table 2. NiO Nanowire Synthesis Results.

Research Group	Nanowire Diameter (nm)	Crystal Structure
Yang et al.	20-60	Hexagonal
Yu et al.	50	Cubic
Cao et al.	150	Cubic

In 2005, Yang et al. [28] reported the synthesis of NiO through a sol-gel process. Nickel nitrate hexahydrate was mixed with citric acid and ethanol. The mixture was then evaporated until a green paste formed, which was heated at 750 °C for 8 hours.

Hexagonal NiO nanowires with 20-60 nm diameters were formed. The authors had no satisfactory explanation of how these nanowires formed but ruled out the vapor-liquid-solid (VLS), vapor-solid (VS) and solid-liquid-solid (SLS) mechanisms.

In 2006, Yu *et al.* [35] reported a templated sol-gel method to grow NiO nanowires. They fabricated their own AAT and used this to grow nanowires. They made templates with varying pore diameters ranging from 30 nm to 60 nm. To make the sol, an aqueous mixture of nickel nitrate hexahydrate and citric acid was prepared. After evaporation of the water, the template was immersed for either 1 minute or 2 minutes and then heated to 500 °C for 1 hour. The authors found that below an immersion time of 1 minute, hollow nanotubes were formed, while above 1 minute, nanowires formed. The structure of the NiO nanowires was cubic.

Another group of researchers also created a templated sol-gel synthesis of NiO nanowires. Cao *et al.* [36] used nickel nitrate hexahydrate, hydrazine and ethanol to create the sol and allowed it to hydrolyze for 5 hours at room temperature. The commercial templates used (Whatman, 100 nm quoted pore diameter) were immersed in the sol for 5 hours then annealed at 600 °C for 5 hours in an argon atmosphere. The nanowires obtained were single-crystalline and had a cubic structure. Although the templates were quoted with 100 nm pore diameter, the authors found through SEM that the pores ranged from 100 to 300 nm in diameter, resulting in an average nanowire diameter of 150 nm.

The three methods discussed above were successfully used to synthesize NiO

nanowires using nickel nitrate hexahydrate with citric acid or hydrazine. The

temperatures employed ranged from 500 °C to 750 °C, and the annealing time ranged

from 1 hour to 8 hours. Yu *et al.*'s method is the most straightforward, having the lowest

annealing temperature as well as the shortest annealing time. Furthermore, the use of

citric acid as opposed to hydrazine is attractive from a safety point of view. Although

Cao *et al.* reported NiO nanowires as well, they did not use a template to control diameter

nor offer any helpful information to understand the growth.

2.3.2 α-Fe₂O₃ Nanowire Synthesis

A limited number of articles have demonstrated growth of hematite (α-Fe$_2$O$_3$)

nanowires synthesized using the sol-gel method. Table 3 shows the synthesis conditions

for the nanowires, and Table 4 shows the results of the synthesis.

Table 3. α-Fe₂O₃ Nanowire Synthesis Parameters.

Research Group	Materials	Template	Heating Conditions
Lin *et al.* (2004)	iron (III) nitrate and 2-methoxyethanol	AAT 60 nm	After electrodeposition 600 °C 24 hours
Suber *et al.* (2005)	iron (III) acetyle acetonate, citric acid and ethanol	AAT 200 nm	60 °C, 4 hour 100 °C, 4 hour 400 °C, 12 hour 600 °C, 12 hour

Table 4. α-Fe$_2$O$_3$ Nanowire Synthesis Results.

Research Group	Nanowire Diameter (nm)	Crystal Structure
Lin *et al.*	60	Hexagonal
Suber *et al.*	200 nm nanotubes of 100 nm nanoparticles	Hexagonal

Lin *et al.* [22] used sol-gel electrophoretic deposition to create dense 50 nm α-Fe$_2$O$_3$ nanowire arrays in alumina templates. The sol was grown from iron (III) nitrate dissolved in 2-methoxyethanol with the pH adjusted between 2 - 3. The mixture was stirred for 2 hours at 60 °C. An alumina template with a gold substrate was used as the cathode and a platinum sheet was used as the anode. Electrodeposition was carried out at 5 V. After electrodeposition, the substrate was annealed at 600 °C for 24 h to crystallize the nanowires. The authors performed optical studies and determined the nanowires exhibited a blue shift with respect to bulk α-Fe$_2$O$_3$, presumably from the quantum size effect.

Suber *et al.* [37] made a number of iron oxide nanowires as well as nanotubes. For α-Fe$_2$O$_3$ nanowires, they utilized both a templated (porous alumina) sol-gel as well as a templated (polycarbonate) particle precipitation - reflux method. The particle precipitation - reflux method created nanowires heterogenously composed of both α-Fe$_2$O$_3$ and β-FeOOH and was poorly crystallized. For the sol-gel method, iron (III) acetyl acetonate and citric acid were dissolved in ethanol. The 100 nm or 200 nm

diameter template was left overnight in solution until gelation. The template was then heated to 60 °C for 4 hours, then 100 °C for another 4 hours and then 400 °C for 12 hours before ramping down to 25 °C. This procedure produced nanowires[†] when 100 nm templates were used and nanotubes when 200 nm templates were used. The authors state that simply increasing the reaction time would be enough to form nanowires in the 200 nm template. The resulting nanowires and nanotubes however, were amorphous. Repeating the procedure with the 200 nm template and adding an additional annealing step of 600 °C for another 12 hours resulted in the formation of α-Fe_2O_3. However, the TEM analysis on the α-Fe_2O_3 nanotubes show that they are not dense but powdery and are composed of spherical particles of about 100 nm in diameter.

Lin *et al.*'s procedure was successful and produced hematite nanowires. However, it is more complicated than Suber *et al.*'s sol-gel procedure which did not require electrodeposition. Although the latter's procedure did not produce dense hematite nanowires, employing a longer evaporation time during the gel formation as advised by the authors may help the formation of nanowires as opposed to nanotubes.

2.4   Sol-Gel Synthesis of Carbide Compounds

To produce carbide materials using a sol-gel route, carbothermal reduction is usually employed. Carbothermal reduction is the formation of a non-oxide ceramic from the reaction within a mixture of carbon and metal-oxides. Silicon carbide is the most

---

[†] Suber *et al.* describe these as nanofibrils rather than nanowires.

investigated carbide compound, followed by titanium carbide, and marginally, zirconium carbide. In general, the overall reaction for the carbothermal reaction of these carbides is as follows:

$$MeO_2 \text{ (g)} + 3C \text{ (s)} \rightarrow MeC \text{ (s)} + 2CO \text{ (g)} \qquad \text{Equation 4}$$
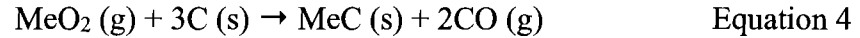
where Me signifies Si, Ti or Zr. For simplicity, only silicon carbide synthesis will be discussed, as the methodology for creating the other carbide compounds is similar.

As is typical for oxide compounds, metal alkoxide precursors are used to create the gel matrix composed of metal-oxygen bonds. For silicon carbide, silicon sources have typically been tetraethoxysilane (TEOS) or methyltriethoxysilane (MTES), although other chemicals have been used. There are two ways of obtaining the carbon necessary for the carbothermal reaction; either the carbon source is internal to the sol mixture, meaning that carbon is incorporated in the gel matrix, or it is external, meaning that a macrostructured carbon source (e.g. char) could surround the sol or other carbon sources are ground up and mixed into the sol (e.g. activated carbon).

2.4.1 Silicon Carbide Sol-Gel Synthesis Using Internal Carbon Sources

In 1993, Seog *et al.* [58] reported on an acid-catalyzed and base-catalyzed sol-gel preparation of silicon carbide spheres. The silicon sources were phenyltrimethoxysilane (PTMS) or a mixture of PTMS and TEOS. The carbon source is contained within PTMS. The acid-catalyzed method produced polydisperse SiC powder whereas the base-catalyzed reaction produced monodisperse SiC powder.

In 1995, Raman et al. [59] reported the effect of using various silicon alkoxides and carbon sources to make SiC. The silicon alkoxides used were TEOS, MTES and a mixture of the two. The carbon sources used were phenolic resin, ethylcellulose, polyacrylonitrile (PAN) and starch. Various gels were prepared, and these were aged, dried and carbonized at 800 °C under argon and then heated to 1550 °C under argon for 2 hours. The mixture that used phenolic resin as the carbon source had the largest degree of crystallinity as determined by x-ray diffraction.

Hasegawa et al. [60] mixed TEOS (silicon source) and dissolved phenolic resin (carbon source) under acidic conditions and annealed the gels at 1500 °C for 2 hours to create SiC fibers. The authors investigated the effect of the carbon to silicon ratio (1.6 to 5.4) by varying the amount of phenolic resin used and determined that SiC fibers could be obtained when the carbon to silicon ratios were 2.6 and above.

2.4.2 Silicon Carbide Sol-Gel Synthesis Using External Carbon Sources

In 1994, Cerovic et al. [61] published their findings on the synthesis of β-SiC powders using sol-gel derived SiO_2 and either activated carbon or succharose as the carbon source. Heating was performed at 1550 °C for 3 hours under argon flow. The effect of the addition of the carbothermal reduction catalyst, boric acid, on the sols was investigated. They found that a C to Si ratio of 3 was optimum when activated carbon was used and 4 when succharose was used. Boric acid improved the yield and crystallinity of the SiC product. A concentration of 3 to 11 wt% boric acid was optimal

for the succharose system, and of 2.4 to 8.1 wt% boric acid was optimum for the activated carbon system.

Raman *et al.* [62] used rayon fibers soaked with sol-gel derived SiO_2 and pyrolyzed at 1400 °C to create SiC whiskers. The silicon sources include phenyltriethoxysilane (PTEOS), dimethyldiethoxysilane (DMDEOS) and TEOS. Rayon was the carbon source. The resulting whiskers were reported as straight, with an aspect ratio of 100 or greater for all samples except when DMDEOS was used.

Rambo *et al.*, [63] who used wood as a template to make complex structures of various carbides, offers an example of template directed sol-gel synthesis of carbides. Pine wood was pyrolyzed at 800 °C to create biocarbon that still maintained the pore structure of the wood. The sol was then vacuum infiltrated into the wood structure where it was dried and then again heated to 1600 °C for 1 hour under an argon atmosphere to produce biomorpic SiC ceramics.

2.5   Sol-Gel Synthesis of Silicon Carbide Nanowires

While there are a number of researchers who have made silicon carbide nanowires using a variety of methods, there are only a few researchers who have made it using the sol-gel method. So far, no one has reported synthesizing silicon carbide nanowires using a template directed sol-gel method. Table 5 summarizes the SiC nanowire synthesis parameters of various researchers using the sol-gel method; Table 5 summarizes the experimental results.

Table 5. SiC Nanowire Synthesis Parameters with TEOS.

Research Group	Materials	Heating Conditions
Meng et al. (2000)	Carbon np	1650 -1800 °C, 2 h, Ar
Li et al. (2001)	Carbonaceous sol	1000 -1500 °C, 1 h, Ar
Jin et al. (2003)	Alumina Sol Phenolic Resin	1200 - 1300 °C, 20 h, Ar
Liang et al. (2000)	Activated carbon Iron np	1650 -1800 °C, 2 h, H_2
Gundiah et al. (2002)	Activated carbon; Ethylene glycol and citric acid	1360 °C 4 or 7 h NH_3 or H_2

Table 6. SiC Nanowire Synthesis Results.

Research Group	Nanowire Diameter (nm)	Crystal Structure
Meng et al.	20-70 15-30	β-SiC + SiO_2 shell β-SiC
Li et al.	15-80	β-SiC + α-SiC
Jin et al.	15	β-SiC + SiO_2 shell
Liang et al.	10-30	β-SiC with SiO_2 shell
Gundiah et al.	350 and 40 (NH_3); 325 (H_2) 750 (NH_3)	β-SiC

In 1999, Meng et al. [64] synthesized β-SiC using sol-gel derived silica with carbon nanoparticles as the carbon source. The gels, when heated to 1650 °C for 1.5

hours and then to 1800 °C for 30 minutes under an argon atmosphere, produced β-SiC

with a SiO_2 shell, whereas the gels heated to 1650 °C for 2.5 hours contained only β-SiC

nanowires.

In 2001, Li *et al.* [65] prepared β-SiC nanowires (the authors used the term

nanowhiskers) using carbonaceous silica aerogels obtained using carbonaceous sol as the

carbon source and TEOS as the silicon source. The gels were annealed between 1000

and 1500 °C under an argon atmosphere for 1 hour. Between 1000 to 1200 °C, the gels

were amorphous. The degree of crystallinity of the wires improved with increasing

annealing temperature.

Jin *et al.*, [27] in 2003, postulated that since aluminum silicate created cage-like

structures, it was possible that a gel containing carbon, aluminum and silicon would

create thinner nanowires, as the cage structure would restrict the size of the nanowires.

The gels were dried and heated between 1200 and 1300 °C for 20 hours in an argon

atmosphere. The resulting products were mostly SiC agglomerates with some nanowires

around 15 nm [27]. The authors claim that the agglomerates were composed of

nanowires [27]. Except for Meng *et al.*, [66] the researchers noted above successfully

created β-SiC nanowires, but the wires had a core shell structure with the crystalline

phase at its core, and an amorphous SiO_2 shell surrounding the nanowire.

Other researchers were able to produce β-SiC nanowires without the amorphous

SiO_2 shell. Liang *et al.*, [66] in 2000, used a ternary sol-gel method using sol-gel derived

silica, activated carbon and iron nanoparticles, reacted and heated at 1400 °C in a reducing H_2 atmosphere as opposed to the typical inert atmosphere.

Gundiah et al., [67] in 2002, created β-SiC nanowires using a variety of methods including the sol-gel methods using TEOS, with activated carbon and 48 % hydrogen fluoride (HF); and TEOS with ethylene glycol and citric acid. These mixtures were then heated in either an H_2 or NH_3 atmosphere at 1360 °C for 4 or 7 hours. Both the sol-gel methods listed above produced β-SiC nanowires. Longer heating times improved the crystallinity of the nanowires. Using the 7-hour heating time and using NH_3 as the reducing atmosphere, the first sol-gel method produced wires with 40 nm while the second method produced wires 750 nm. The authors note that the second method produced straight growth. The experiment using an H_2 atmosphere with a 7-hour heating time applied to the first sol-gel method only and produced wires with 325 nm [67].

From this body of research, it appears that whether the carbon source is internal or external, the synthesis of silicon carbide is a simple matter of bringing an appropriate amount of carbon, silicon and oxygen together and then annealing the mixture at an appropriate temperature in an inert or reducing atmosphere. The work performed by Rambo et al. is the closest model there is of a template-directed synthesis given the use of pyrolyzed wood as the mold, suggesting that template based morphological control of synthesized SiC is feasible. Although there has been success in growing silicon carbide nanowires using the sol-gel method, these methods have not demonstrated the ability to control the nanowire's diameter.

2.6 Summary of Template Directed Sol-Gel Growth of Nanowires

Nanowire oxides have been successfully grown by the sol-gel template directed method. Silicon carbide nanowires have been made using sol-gel techniques using a variety of carbon sources. However, silicon carbide nanowires have not been made using the sol-gel template-directed method. In this thesis, fabricated as well as commercial templates were used to grow oxide nanowires. These nanowires were characterized for morphology, composition and structure. In the case of carbide nanowires, there is currently no process to control the dimensions of the nanowires. Growth of silicon carbide nanowires using templates was attempted in this thesis work.

CHAPTER THREE

EXPERIMENTAL METHODS AND MATERIALS

3.1   Objectives

The objectives of this study were as follows:

1) Fabricate porous alumina template at room temperature and 0 °C to determine what

effect temperature has on the pore features.

2) Synthesize NiO and α-Fe$_2$O$_3$ nanowires with varying diameters using template

directed sol-gel synthesis.

3) Synthesize SiC nanowires using the template directed sol-gel synthesis method.

3.2   Fabrication of Porous Alumina Templates

To fabricate porous alumina templates, a double walled cylindrical

electrochemical cell was used, as shown in Figure 2. The inner cylinder is open on both

ends. An o-ring is attached to the bottom end of the inner cylinder, which is used to form

a seal around the aluminum substrate to be anodized. To adjust the anodizing

temperature, the outer cylinder, which has an inlet port and outlet port, is used to

continuously circulate temperature controlled liquid. A platinum wire served as the

cathode. An Agilent E3612A power supply was used as the DC power supply. In a

typical experiment at room temperature, an approximately 2 x 1 inch strip of 99.9995 %

aluminum foil was sonicated in methanol or acetone for 10 minutes and rinsed in

deionized water. The foil was dried with lint free tissue and then attached to the bottom

of the inner cylinder. The cylinder was filled with 0.3 M oxalic acid electrolyte
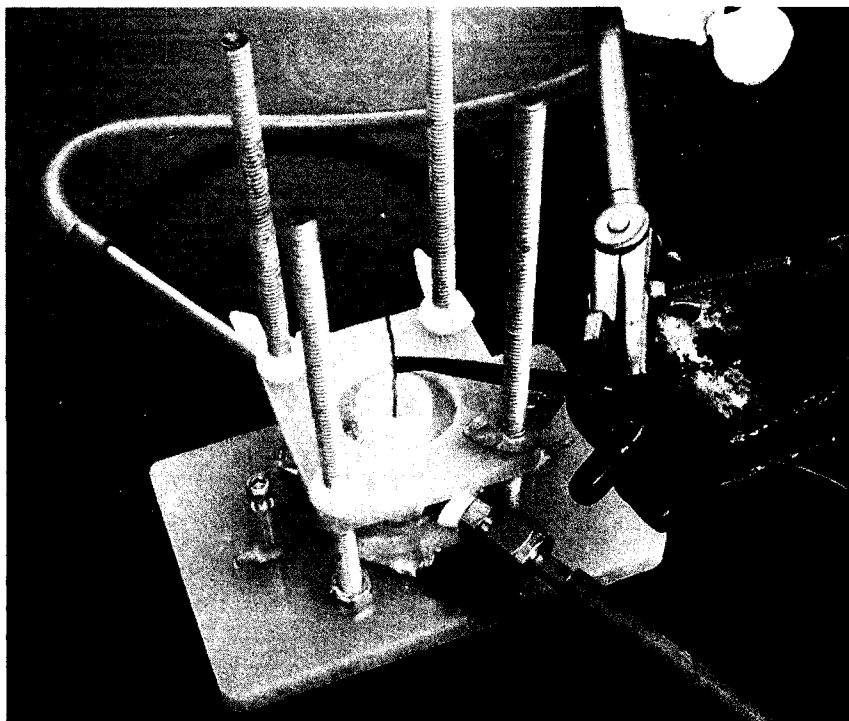
Figure 2. The anodization cell used in this work.

solution. The cathode was dipped into the solution while the aluminum foil was attached

to an electrode to serve as the anode. The first anodization was conducted at 40 V.

Etching of the first alumina layer was conducted at room temperature for 3 hours in 0.4

M phosphoric acid. The second anodization was conducted at the same conditions as the

first anodization, except the anodizing time ranged between 30 minutes and 2 hours.

Varying the second anodization time varies the pore length. For analysis of pore

development, shorter second anodization times were used. For use in nanowire growth or

if detachment of the template from the aluminum was performed, longer second

anodization times were used.

The fabrication of porous alumina templates at cold temperature was similar to

room temperature anodization except ice water was circulated through the outer cylinder

15 minutes before anodization and throughout the first and second anodization process. Also, due to slower kinetics, the duration of the second anodization was extended to 4 hours. A flow diagram of the anodization process is provided in Figure 3. If detachment of the alumina membrane was performed, then a pulse at 50 V using a 1:1 solution of ethanol and 78% perchloric acid was delivered to the substrate, as described by Chen *et al.* [55]. After fabrication, the templates were characterized by SEM as described in Section 3.6.

Aluminum foil •——

First chemical anodization

Alumina with
uneven pores •——

Etching

Alumina etched away •——

Second chemical anodization

Alumina with
even pores •——
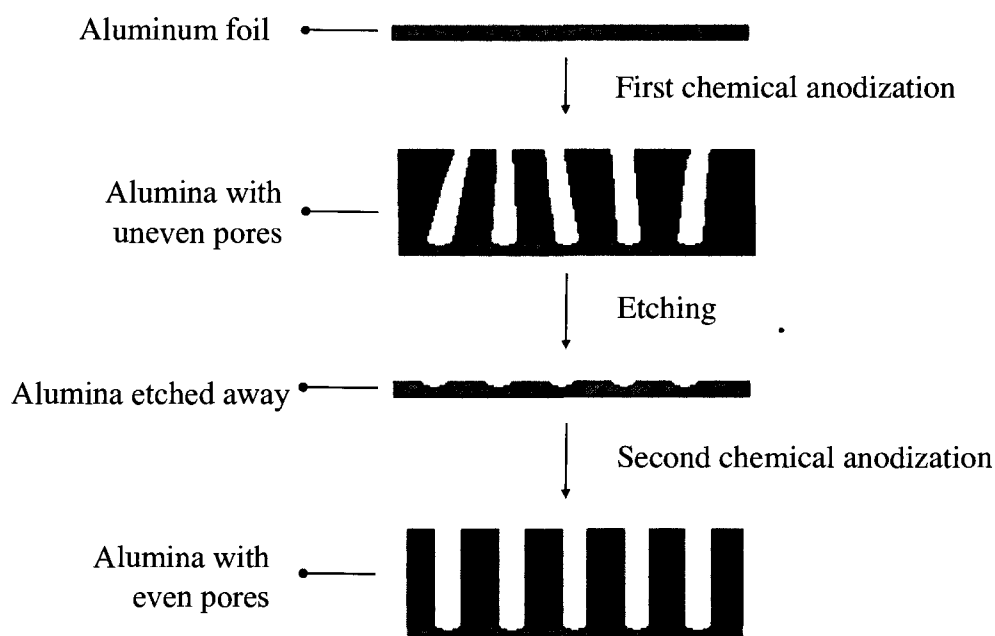
Figure 3. A flow diagram of alumina template synthesis.

3.3   Annealing of Commercial Templates

The commercial templates (Whatman, Anodisc 13, 200 nm pore diameter) were annealed to determine the effect of temperature on the crystal structure of the templates. The templates were placed in a quartz tube and annealed in a Lindberg Blue M tube

furnace for 3 hours at either 600 °C or 900 °C after ramping up at 10 °C/min. These

templates were characterized using XRD as discussed in Section 3.6.

3.4   Nanowire Synthesis Procedures

Figure 4 gives a schematic of the nanowire synthesis procedure, which involves

the following steps: precursor selection, sol synthesis, template immersion, gel formation

and annealing.
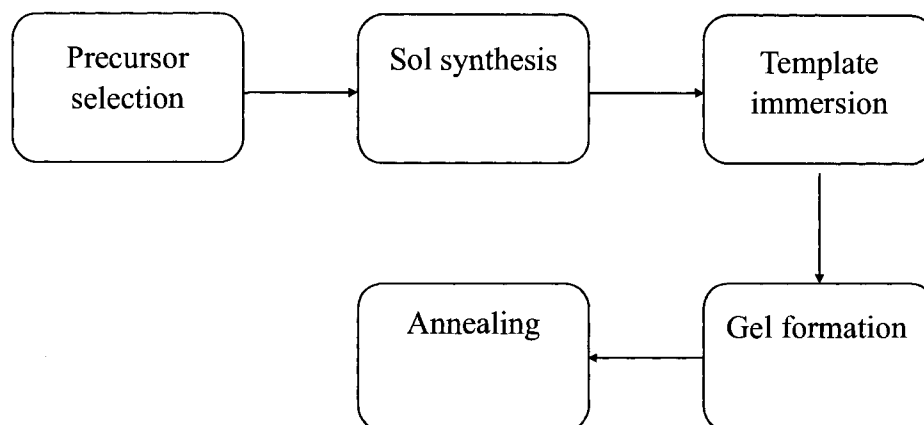
Figure 4. A flowchart for synthesizing nanowires using the sol-gel template
directed procedure.

Precursors for sol-gel chemistry are usually either metal salts or metal organic

compounds, the most popular of this class being the metal alkoxides. Other materials

such as catalysts or chelating agents may be added to hasten gel formation.

After the selection of the precursor, the sol is synthesized. The chemicals added

need to be given time to proceed with the polymerization to form the sol. The solution

will increase with viscosity over time. It is important in this phase of synthesis that

enough time is given for the reaction to proceed and form sol particles, but not so much

time that the sol becomes too viscous to allow infiltration into the pore structure of the template.

Once an appropriate amount of time has passed for sol formation, the template, whether fabricated or commercial, is immersed. The amount of time that the template is immersed is also important. Taking the template out too soon may result in the formation of nanotubes instead of nanowires.

Before the template is annealed, it is left to dry to allow the polymerization reaction to proceed to completion and drive out the solvents. Depending on the system, this step may occur at elevated temperature or room temperature.

The final step of the synthesis procedure is to anneal the gel-containing template. A tube furnace, shown in Figure 5, was used for the annealing stage.
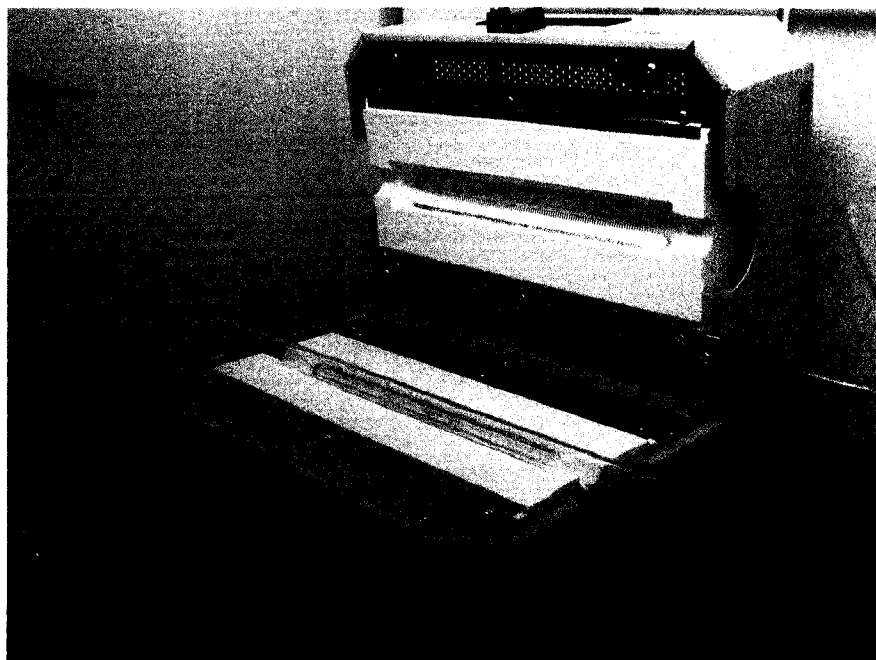
Figure 5. The tube furnace used in this work.

The parameters to consider include annealing temperature, atmosphere (e.g. inert or reducing) and annealing time. The formation of ceramics usually requires high temperatures. For example, the temperature needed to form NiO is around 500 °C [35]. For SiC, temperatures between 1200 °C and 1800 °C are required [58-67]. On some materials, it may also be important to control the atmosphere. For example, if oxygen needs to be driven off from the gel, an inert atmosphere may be necessary to minimize exposure to oxygen. Upon completion of the synthesis, the templates were prepared as required for analysis.

3.4.1 Nickel (II) Oxide Nanowire Synthesis

The procedure by Yu *et al.* [35] was used for synthesizing NiO nanowires. It is so far the simplest method and has demonstrated success in making nanowires using the template directed sol-gel method.

In this method, 2.10 g citric acid was dissolved in 50 mL of deionized water heated to 80 °C. In another beaker, 11.63 g of nickel (II) nitrate hexahydrate was dissolved in room temperature deionized water. The two solutions were combined and stirred for 30 minutes at 80 °C. The mixture was left to evaporate until about 1/2 to 1/4 of its volume remained[†]. An alumina template was dipped into the mixture for 2 minutes and excess material was carefully blotted from the template using lint free tissue. The templates were left to dry for an hour and then annealed in a quartz tube furnace at 500°C

---

† This is a slight deviation from the original procedure, where the liquid is completely driven off.

for 1 hour. The heating rate was 10 °C / min. NiO on the template surface was removed by polishing it off with 1200 grit sandpaper.

3.4.2 Hematite Nanowire Synthesis

The procedure by Suber *et al.* [37] was used for synthesizing hematite nanowires. In this method, 0.0881g of iron (III) 2, 4 pentanedionate and 0.192 g citric acid was dissolved in 50 mL of ethanol. The solution was stirred for 15 minutes. After stirring, a template was placed in the solution and was left under a hood overnight to evaporate at room temperature. To ensure that nanowires instead of nanotubes would be produced, the mixture was evaporated to the extent that it would no longer flow. The viscosity made it difficult to extract the template, which sometimes got stuck at the bottom of the beaker. In this case, ethanol was added, drop wise, around the template to help gently pry it off. It was then dried immediately on lint free tissue. As the template is surrounded by a thin film of the gel at this stage, it is unlikely that the gel in the pores were dissolved by this process. Once the template was removed, it was placed in a quartz tube furnace and heated in air at 60 °C for 4 hours, then 100 °C for 4 hours, 400 °C for 12 hours and finally 600 °C for 12 hours. The film surrounding the template was removed using 1200 grit sandpaper.

3.4.3   Silicon Carbide Synthesis

Two sol-gel carbothermal reduction formulas, one from Hasegawa *et al.* [60] and one from Gundiah *et al.* [67], were investigated.

Hasegawa *et al.*'s procedure [67] with some modification is described as follows: 2 g of novelac-type phenolic resin was dissolved in 10 mL ethanol, 15 mL tetraethylorthosilicate (TEOS) and 2.42 mL of 0.3 M hydrochloric acid (HCl). The mixture was stirred for 5 minutes. After stirring, the mixture was left to stand at 65 °C. The clear color of the mixture changes to pale yellow then darkens to peach then orange. The template was dipped in in the mixture for 2 minutes when the mixture just turned orange and the viscosity resembled thinned honey. Excess material on the template surface was removed with lint free tissue. The template was moved into a quartz tube furnace which was then purged with argon for at least 15 minutes, after which the template was annealed under argon to 1000 °C at a heating rate of 10 °C/min. The dwell time at 1000 °C was 20 hours. This procedure differs from Hasegawa *et al.*'s [60] procedure in two ways. First, the annealing temperature was lower by 500 °C due to lack of access to hotter furnaces, requiring an extended dwell time in the furnace from 4 hours to 6 hours. Second, to grow nanowires, a template was used.

The procedure based on that of Gundiah *et al.* [67] is as follows: 10 mL ethanol and 2 mL TEOS were mixed together for 10-15 minutes. 0.424 g activated carbon and 1 mL of 48% hydroflouric acid (HF) was added. The mixture was stirred continuously for approximately 3 hours and then the template was placed into the mixture for 1 minute. The template was then placed into an alumina crucible and dried in an alumina tube

furnace at 125 °C for 1 hour. The tube furnace was purged with 10% hydrogen in argon gas (H_2/Ar) for at least 15 minutes. The template was annealed under the H_2/Ar gas at 1100 °C[†] for 10 hours. The procedure differs from the original in the following ways: the annealing temperature is 200 °C cooler that that of Gundiah *et al.* [67] and the dwell time is extended to 10 hours instead of 7 hours. A template was utilized. Also, H_2/Ar gas was used instead of pure hydrogen.

3.5 Sample Preparation

For SEM and EDS experiments, the templates were partially dissolved in 6 M sodium hydroxide (NaOH) for approximately 11 minutes and rinsed thoroughly with deionized water. Samples were later gold sputtered as necessary. For XRD experiments, samples were lapped using SiC 1200 grit sandpaper.

3.6 Analytical Techniques

This section describes the analytical techniques used to characterize the templates as well as the nanowires. Section 3.6.1 discusses scanning electron microscopy (SEM). Section 3.6.2 discusses energy dispersive x-ray spectroscopy (EDS) and Section 3.6.3 discusses x-ray diffraction (XRD).

[†] The acquisition of alumina crucibles enabled the operation of the tube furnace to its maximum temperature of 1100 °C instead of 1000 °C.

3.6.1 Scanning Electron Microscopy

To be able to determine the shape and size of the nanowires, electron microscopy was used since nanowires can be between 10 and 100 nm in diameter. For electrons, whose wavelength is smaller than visible light, the theoretical maximum resolution is 0.0021 nm [68]. In practical use however, a scanning electron microscope, depending on type and operating conditions, will have resolution between 10 and 100 nm. A scanning electron microscope uses electrons, analogous to using light for ordinary microscopes, to produce an image. Under vacuum, electrons are generated (thermoionically or by field emission) and accelerated from the electron gun towards the sample. As the electrons travel towards the target specimen, they go through condenser lenses, which focus the electrons electromagnetically into a beam. The beam then moves through scanning coils, which bend the beam in a raster pattern across the sample - the scanning portion for which the technique is named [69]. Figure 6 shows a schematic of an SEM.
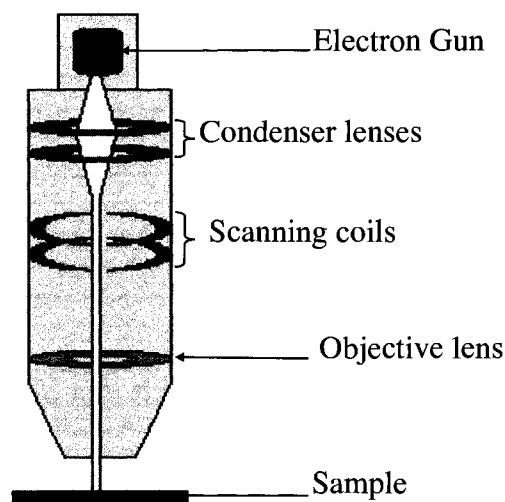
Figure 6. A schematic of a scanning electron microscope.

When the electron beam strikes the sample, it penetrates the sample to a depth which is proportional to the beam intensity and inversely proportional to the sample atomic number. A number of signals are emitted from the sample from the penetrated volume, but for SEM, only secondary and backscattered electrons are collected. When electrons from the beam come out of the sample with most of their original energy, they are called backscattered electrons. Conversely, electrons that are emitted from the sample with very little energy are called secondary electrons. The energy demarcation between a backscattered electron and a secondary electron is 50 eV. The backscattered and secondary electrons are emitted from the sample in all directions. To obtain as much signal as possible, an SEM has a positively charged collector that draws the electrons to the detector, particularly the low energy secondary electrons. The electron signals that are detected are then amplified and transformed into an image [69]. Figure 7 shows an example of an SEM image.

Figure 7. An example of an SEM image. The image shows NiO nanowire bundles.

The FEI Quanta 200 environmental SEM with EDAX in the Materials

Characterization and Metrology Center [MC]² at San Jose State University, as well as an

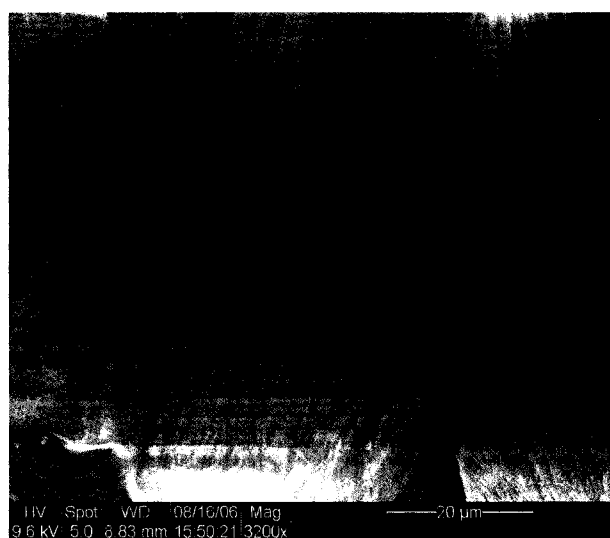FEI XL30 Sirion SEM at the Stanford Nanocharacterization Laboratory at Stanford

University were used for the micrographs taken in this study.

3.6.2   Energy Dispersive X-Ray Spectroscopy

Energy Dispersive X-Ray Spectroscopy (EDS) performs an analysis of the

elemental composition of a given sample. EDS analysis can usually be performed in

conjunction with SEM analysis. As previously mentioned, when an electron beam strikes

the surface of a sample, a number of signals are emitted. Apart from the backscattered

and secondary electrons, characteristic x-rays are also emitted. The electron beam can

knock out electrons from the atoms of the sample. In order for the atom to stay in the

lowest energy state, an electron from a higher energy level replaces the electron that was

knocked out and in doing so, releases x-rays. Since each element has a specific number

of protons, the binding energy that holds an electron to its shell is unique, and the energy

of the x-ray that is emitted upon replacing a knocked out electron is also unique to the

element [69].

EDS nomenclature uses the electron shells of an atom to name the type of x-rays

emitted. The shell closest to the nucleus is termed the K shell, the second the L shell and

the third the M shell, and so forth, as shown in Figure 8.
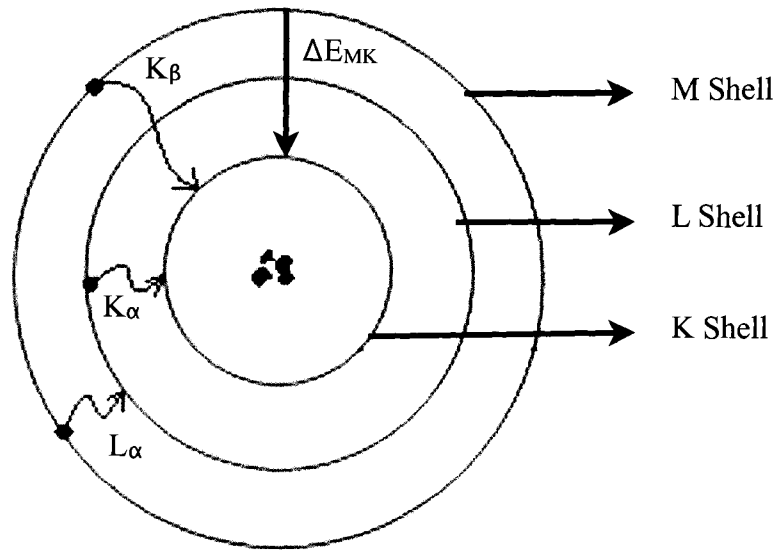
Figure 8. An illustration of an atom with three energy level or "shells". The number of energy levels the electron travelled to fill an empty shell are denoted by the Greek letters. ΔE denotes the difference in energy between two shells which corresponds to the energy of the x-ray emitted.

X-rays are identified by the energy level of the empty shell an electron fills as well as the number of energy levels the electron traveled to fill the empty shell. For a difference in one energy level, the x-ray is α, for two energy levels, β, for three energy levels, γ and so forth. For example, if an M electron replaces a K electron, the x-ray released is called K_β.

The technique is called "energy-dispersive" because the energy of the x-ray is detected through dissipation. The x-rays that find their way into the detector strike a semi-conducting crystal that absorbs the energy of the x-ray. The energy absorbed is turned into an electrical signal, digitized and sorted by energy level. The number of times the crystal absorbs a particular energy level is translated into intensity. The results that

are displayed come in the form of a plot of intensity (KCnt) vs. energy . The

characteristic energies of the elements are known and are contained in a database. The

peaks generated from the plot are compared with the database to identify the element

[69]. Figure 9 shows an example of an EDS spectrum. This technique was used in order

to determine the elemental composition of the nanowires. However, without calibrated

samples, this technique is qualitative only. The FEI Quanta 200 environmental SEM with

EDAX from the Materials Characterization and Metrology Center at San Jose State

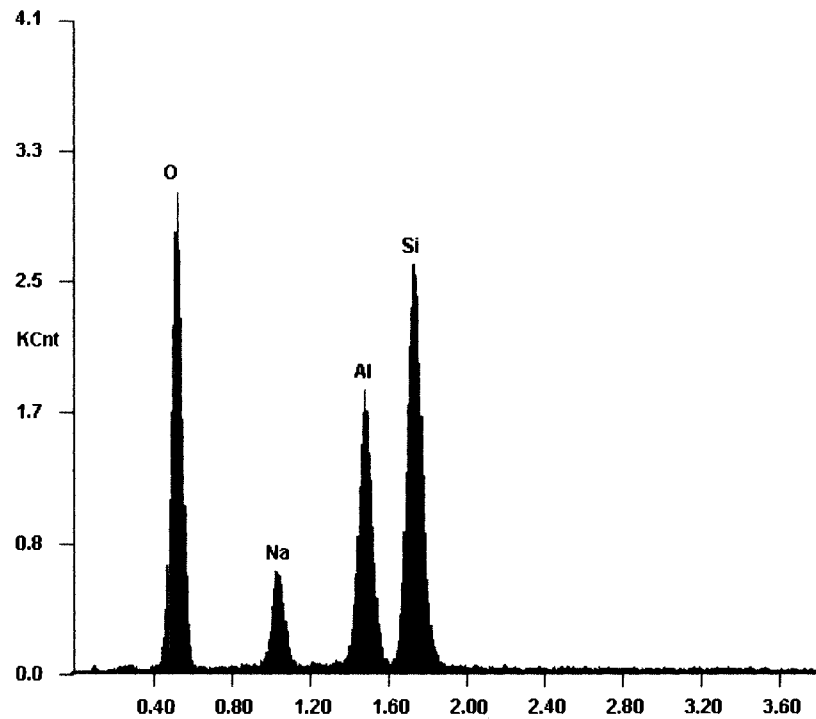University was used for the EDS spectrums obtained for this study.

Figure 9. An example of an EDS spectrum showing Na, Al, Si and O peaks.

3.6.3 X-Ray Diffraction

Elemental analysis is a useful technique to determine chemical composition; however, it cannot determine the material phases present. The combination of EDS and X-ray diffraction may be used to determine the phases present by identifying both the chemical composition and the crystal structure of the nanowire.

When x-rays strike a crystalline substance, they are scattered in all directions. For some directions, the waves will constructively interfere with one another, a phenomenon called diffraction. The combination of constructive and destructive interference leads to diffraction patterns that can be used in conjunction with Bragg's law to determine the crystalline structure of materials [70]. Bragg's law is given by:

$$n\lambda = 2d\sin\theta, \qquad\qquad \text{Equation 5}$$

where n is the order of scattering; λ is the wavelength of the x-ray; d is the spacing between crystalline planes and θ is the angle of incidence and the diffraction angle.

In x-ray powder diffraction, samples are rotated while being struck by a monochromatic beam of x-rays so that the lattice and x-ray beam orientation produces the diffraction pattern. Since lattice planes are oriented in every direction in a random powder, a diffraction pattern from many planes will be created [70]. The data from an XRD experiment is indexed and compared to a library of diffraction patterns to determine the crystal structure and thus identify the phases present. Figure 10 shows a sample XRD diffractogram. The x-axis shows the diffraction angle (2θ) while the y-axis shows the intensity (counts). The Rigaku Ultima III X-Ray Diffractometer in the Materials

42

Characterization and Metrology Center at San Jose State University was used to obtain
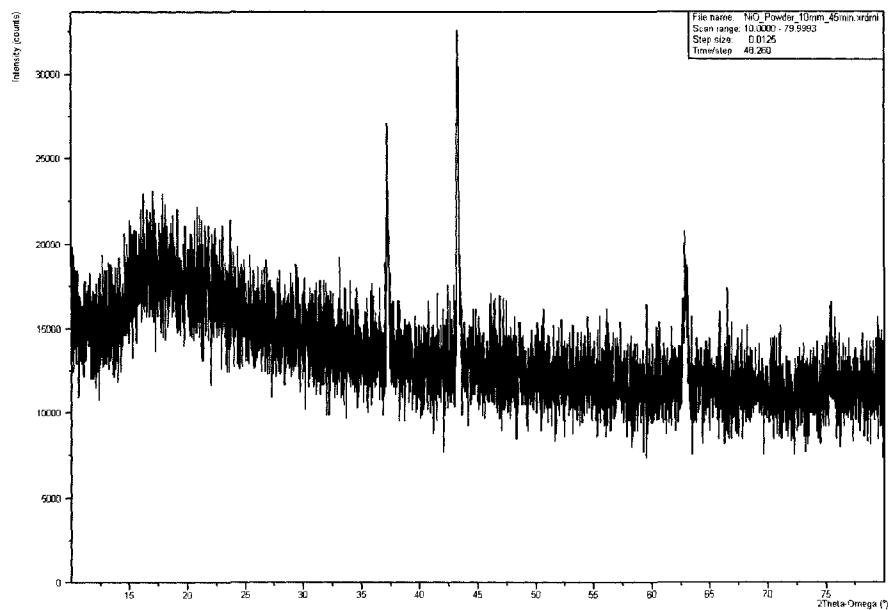
the XRD data in this study.

Figure 10. An example of an XRD diffractogram for NiO powder.

CHAPTER FOUR

EXPERIMENTAL RESULTS AND DISCUSSION

4.1   Results and Discussion

In this chapter, the experimental results as well as a discussion of these results are presented. Section 4.2 focuses on the results of the alumina templates anodized at room temperature as well as at 0 °C. The effect of temperature on the crystal structure of alumina is also discussed. Section 4.3 presents the results of the nickel oxide nanowire synthesis. Section 4.4 presents the results of the hematite nanowire synthesis, and Section 4.5 presents the results of the silicon carbide nanowire synthesis, including the troubleshooting of the alumina template, which presented experimental challenges to the characterization of the silicon carbide nanowires.

4.2   Fabrication of Porous Alumina Templates

This section discusses the results from the experiments conducted in fabricating alumina templates. Section 4.2.1 deals with the room temperature anodization of alumina, showing data at each anodization phase. Section 4.2.2 deals with the anodization of alumina at 0 °C and compares the results with the room temperature anodization. Finally, Section 4.2.3 discusses the crystal structure of commercial alumina when annealed at 600 °C and 900 °C.

4.2.1 Room Temperature Anodization

As previously described, the anodization process consists of three stages: the first

anodization, the etching phase and the second anodization. SEM images of the alumina

template as it progresses through all three processing stages are presented. Figure 11

shows the alumina template after 2 hours of anodization at room temperature. The pores

have developed along strained regions of the aluminum surface and the sample contains

varying pore sizes as well as underdeveloped pores.
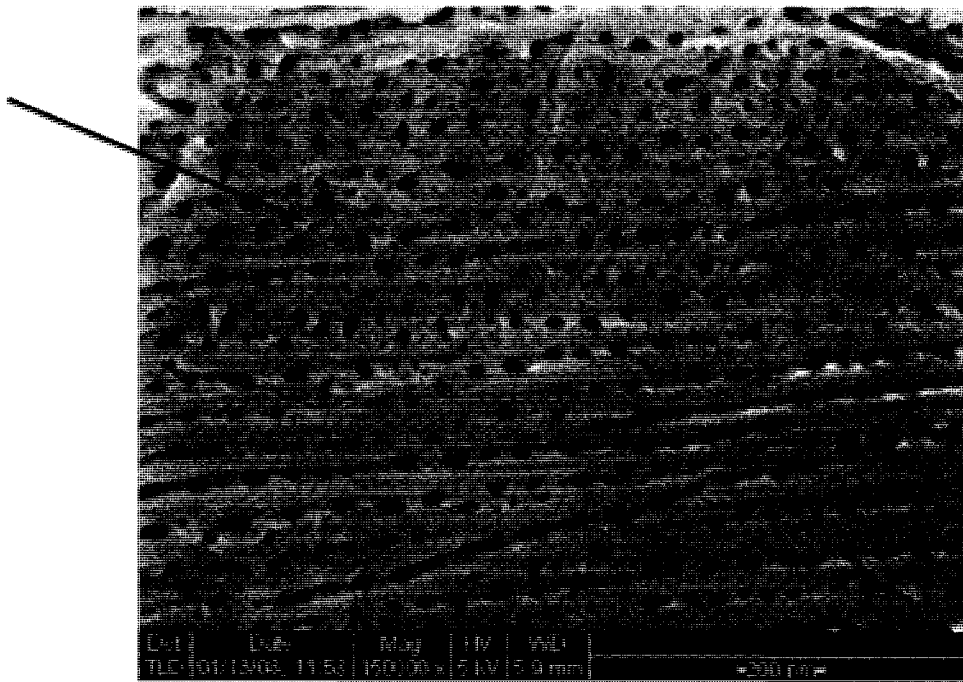
Figure 11. An SEM image of an alumina template after a 2 hour anodization at room temperature. The arrow points to an underdeveloped pore.

Figure 12 shows the alumina template after 3 hours of etching in 0.4 M

phosphoric acid. There are three distinct regions that can be distinguished from the

image. First is the dark flat regions, followed by the clumps of white alumina and finally

the pale white "trails" that seem to surround the clumped regions.
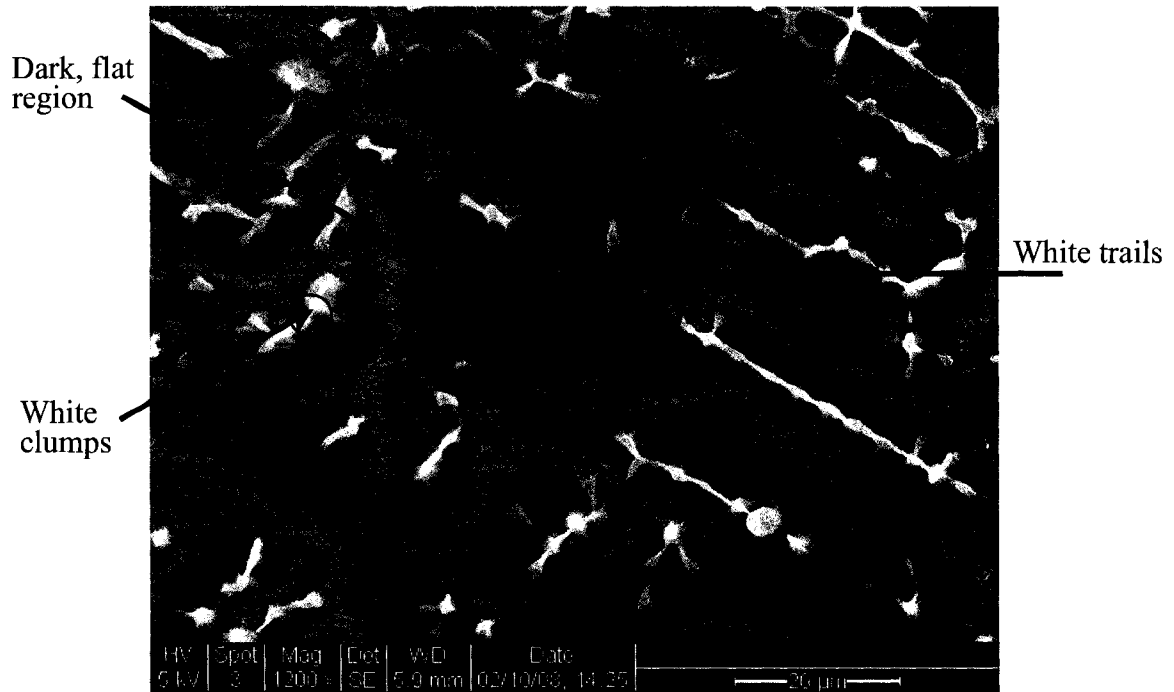
Figure 12. An SEM image of an alumina template after a 2 hour anodization at room temperature and 3 hours of etching. The arrows mark three distinct features on the image: the white clumps, the white trails, and the dark, flat regions.

Figure 13a is an SEM image of the dark flat regions. The area is densely packed

with what appears to be nanowires. Magnification of that region in Figure 13b allows a

visual approximation of about 40 nm for the diameter of the nanowires.
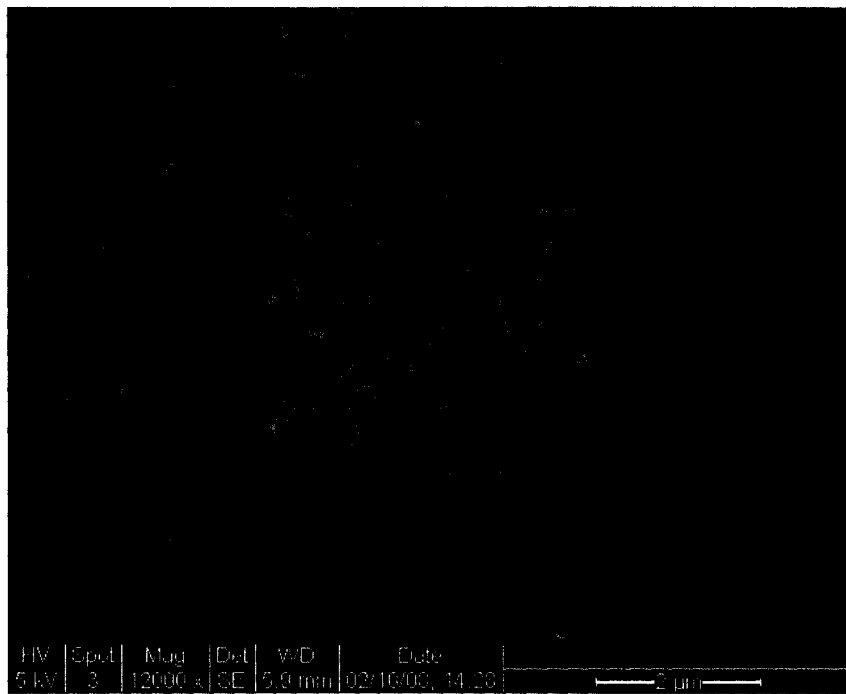
(a)
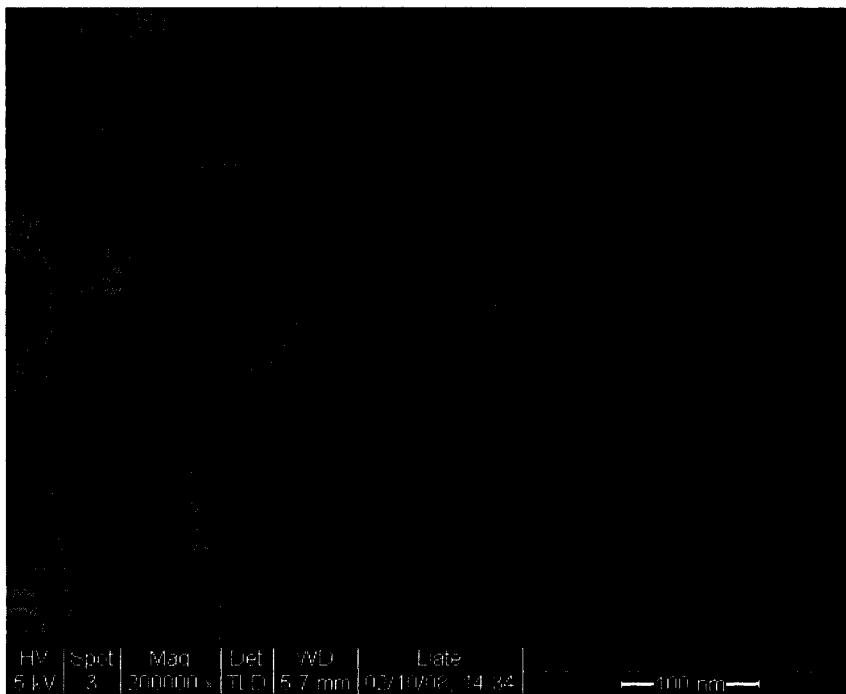
(b)

Figure 13. An SEM image of the dark and flat regions at (a) 12000 x and (b) 200000 x, revealing that the etching phase of the anodization process produces nanowires.

Figure 14 shows an SEM image of the white clumps. It appears that these are simply entangled bundles of nanowires as shown in Figure 13.
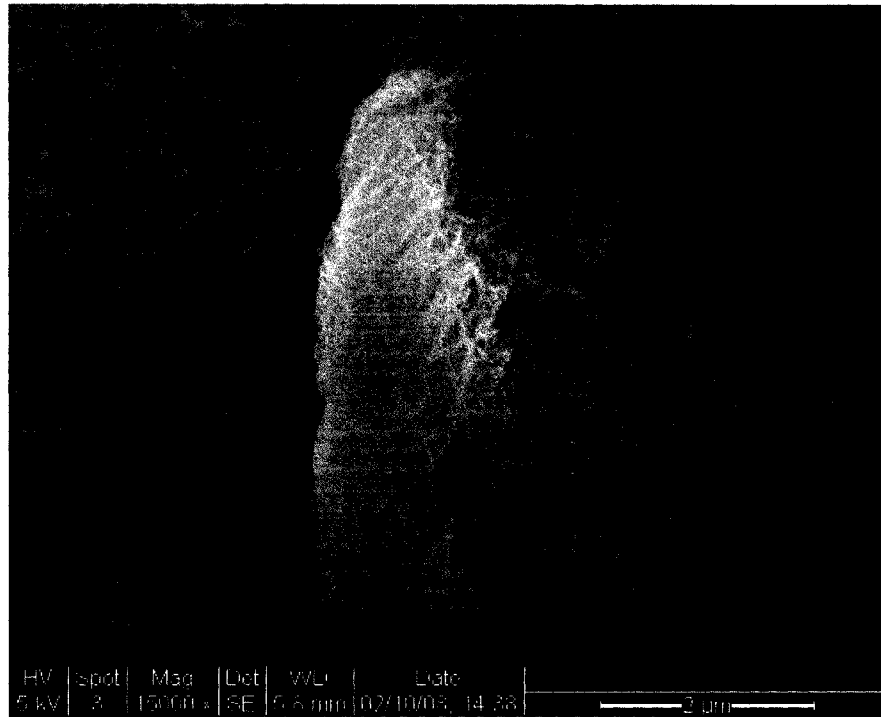
Figure 14. An SEM image of the white bundles found on the alumina template after the etching phase.

Figure 15a focuses on the white "trails" found around the alumina template after etching. The trails are actually the pore imprint on the surface of the aluminum, which are visible on the surface amid the tangle of nanowires surrounding them. Closer inspection of the region in Figure 15b shows the well organized pore formation as well as the scalloped texture of the aluminum metal. It is also apparent from the image that the nanowires are attached and likely grew out of the pore structure.

48
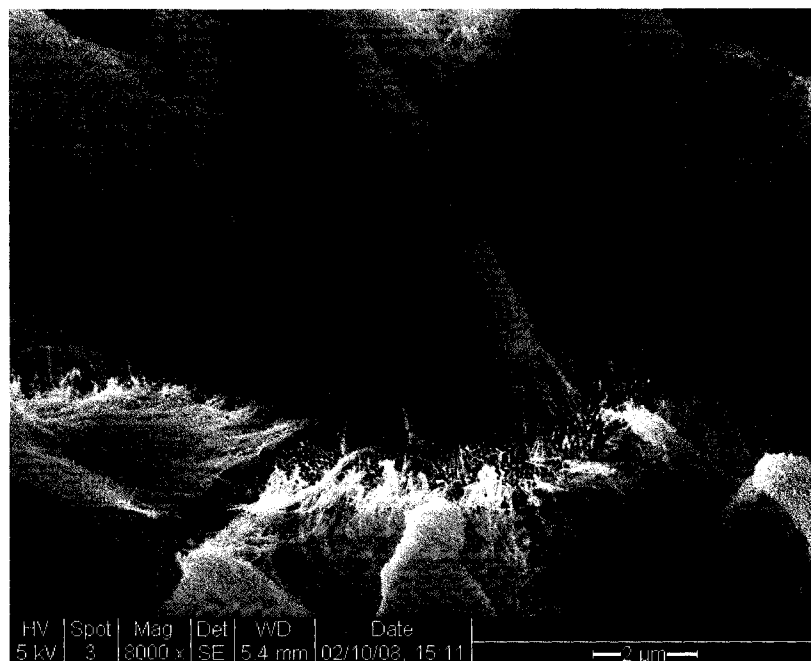
(a)
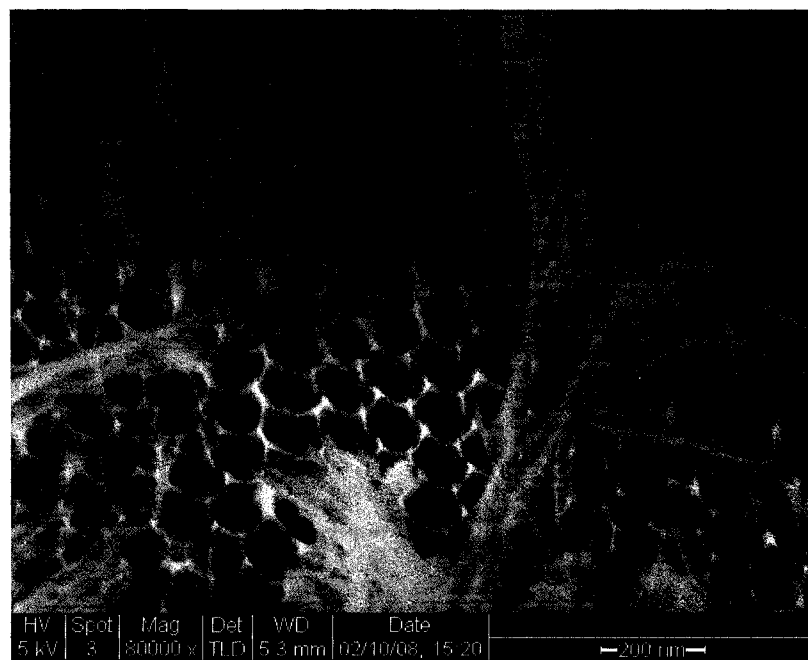
(b)

Figure 15. (a) An SEM image of the white "trails" found on the alumina template after the etching phase. (b) The well ordered and scalloped texture of the aluminum surface is clearly visible.

Figures 16, 17 and 18 show the alumina template after completion of the second

anodization process, which took 35 minutes. Figure 16 shows the low magnification

view of the alumina template. The pores have uniform diameters of around 50 nm and

are arranged in approximately hexagonal patterns. Traces of undissolved alumina

nanowires from the first anodization remain on the surface.
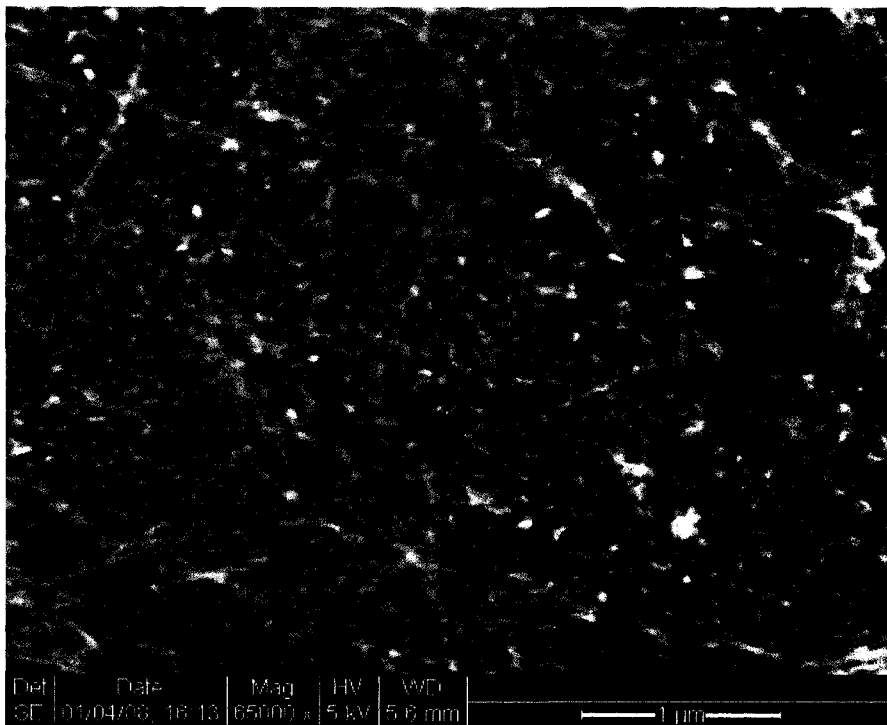
Figure 16. SEM image of alumina template after fabrication process was
completed. The second anodization took 35 minutes.

Figure 17a is an SEM image of the same sample shown in Figure 16, but at a

different region. One can see the that there are still dense layers of nanowires on the

surface. A higher magnification of this region in Figure 17b shows the pores lying

beneath the dense mat of nanowires.
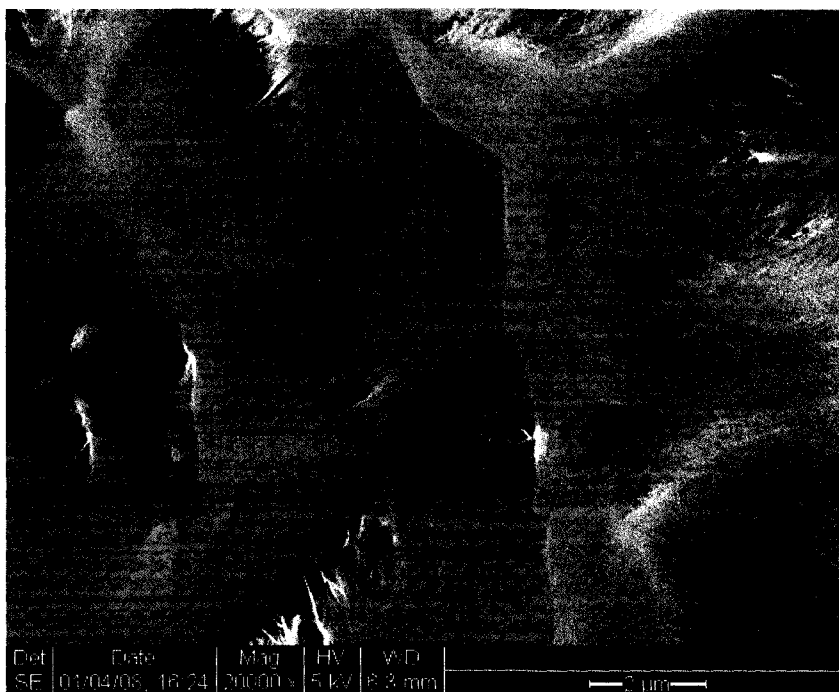
(a)

(b)

Figure 17. (a) An SEM image of a different region on the same alumina template used in Figure 16. (b) The pores are visible beneath the nanowires.

A lengthwise view of the template is shown in Figure 18a. Figure 18b shows the lengthwise view of the templates after treatment in 5 % phosphoric acid for 1 minute. Post treatment with 5 % phosphoric acid was used to improve the visibility of the pore structure, although chemical attack on the pores was also noted.

(a)   (b)
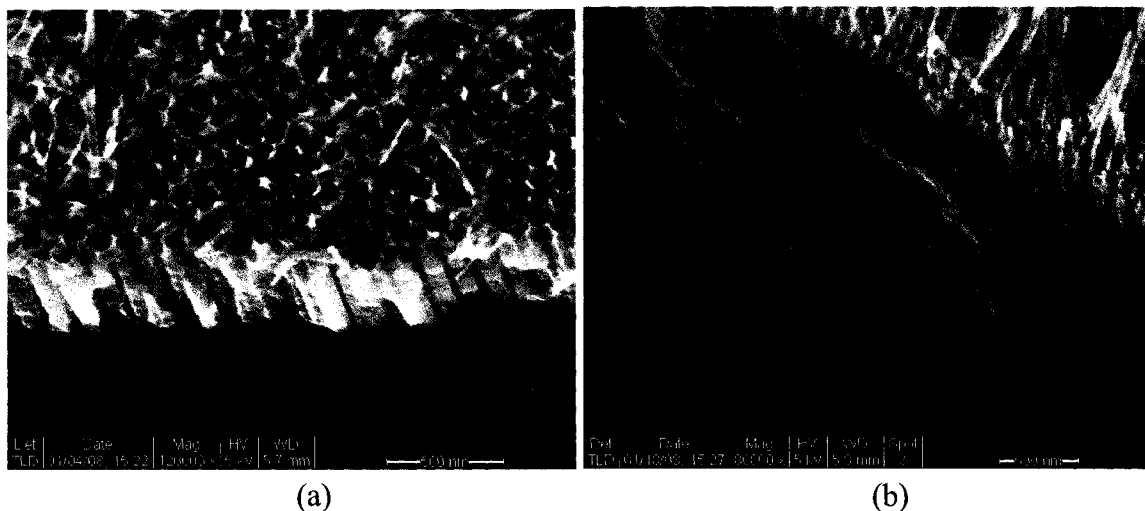
Figure 18. (a) An SEM image of a different region on the same alumina template shown in Figure 16. (b) Image of the pores after post treatment in 5 % phosphoric acid for 1 minute.

The SEM images illustrate the progression of the alumina template from the first anodization to the final anodization. After the first anodization shown in Figure 11, pores on the surface are organized along the strained regions of aluminum and have non-uniform diameters. However, as evidenced by the etched template imaged in Figure 15, the pores at the bottom are hexagonally ordered and retain a scalloped texture. The alumina that grows out the of the second anodization retains the structure and grows hexagonally arranged parallel pores, as shown in Figure 16 and Figure 18. The

observations on the progression of the alumina template are in accordance with the literature. Figure 3 may be revisited for a schematic of this progression.

The presence of nanowires that cover the surface of the template after the etching and the second anodization phase may be partially explained by the chemical attack of the phosphoric acid. After all, that's what it is meant to do. However, the retention of a nanowire morphology is not fully explained simply by chemical attack. A possible explanation may be found in the chemical composition of the pores, as well as the hexagonal ordering of the pores. As explored in Chapter 2.2, it has been observed that the pores are composed of a relatively pure outer alumina layer and an inner ion contaminated layer. Given that phosphoric acid is used in pore widening procedures, it is likely that the contaminated layer is etched much faster than the relatively pure alumina layer. Once the inner layer is etched away, the relatively pure outer layer remains to be etched. The hexagonal organization of the pore cell may contribute to a denser wall at a point than at an edge. It is possible that the difference in wall density also contributes to differences in the time needed to etch away one area over another, allowing the eventual destruction of the overall structure while still retaining the nanowire shape. More research is needed to verify this hypothesis. Figure 19 shows a schematic of the proposed etching behavior.
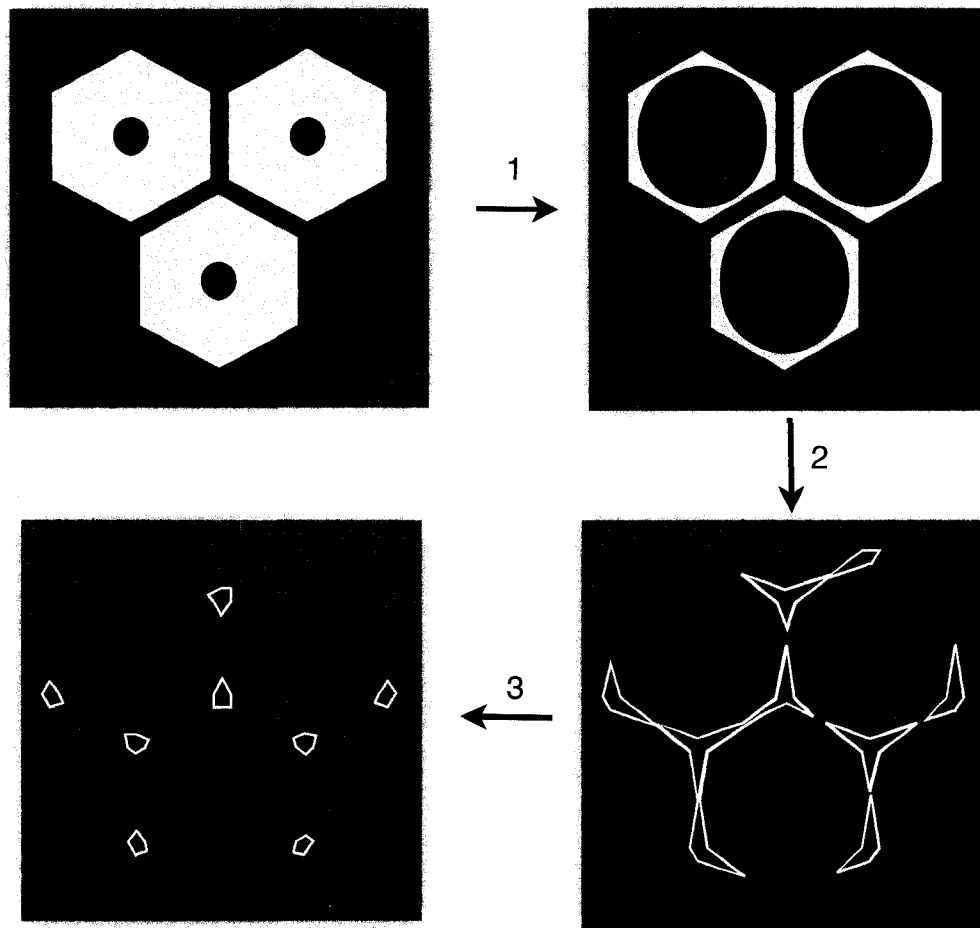
Figure 19. A cross-sectional schematic of hexagonally arranged alumina pores dissolving to form nanowire residues. The inner layer is dissolved first, then the hexagonal edge which may have a smaller density, leaving the points on the hexagonal structure.

The nanowires do illustrate, however, that the etching process as it currently stands is not completely effective in removing the alumina layer produced by the first anodization.

Another template that was fabricated through the entire process (second anodization duration of 1.75 hours) and detached from the aluminum is shown in Figure 20. Because of the detachment process, the second anodization ran longer than 35

minutes and shorter than 2 hours to ensure a sturdy template while still maintaining an aluminum backing. Although stray nanowires are evidenced in the template, uncluttered regions such as the one shown in Figure 20a are more readily found. The higher magnification in Figure 20b shows pore diameters of around 50 nm and interpore distances of around 115 nm.

(a)   (b)
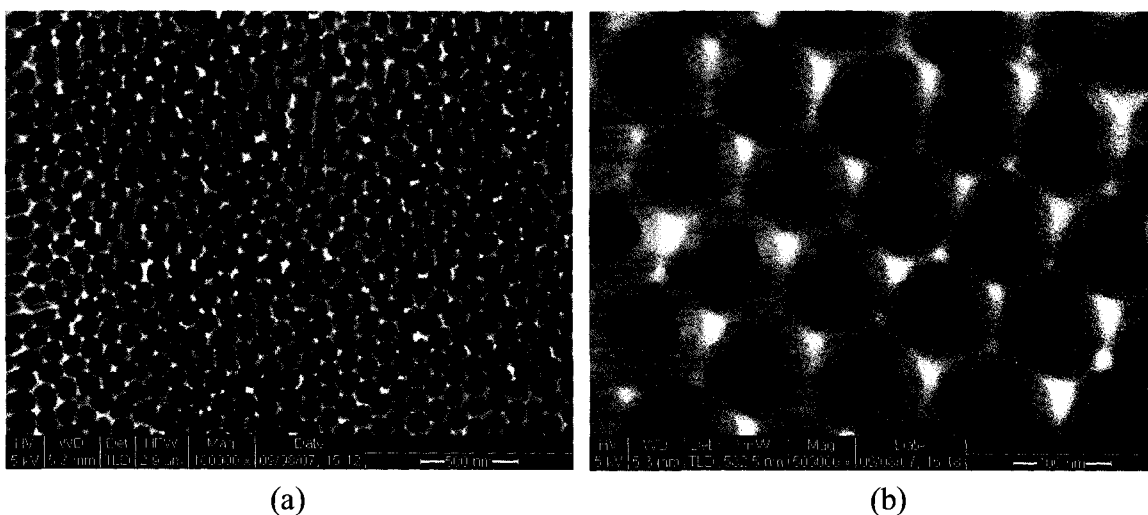
Figure 20. An SEM image of template after room temperature anodization at (a) 100000 X and (b) 500000X.

The reduction in the number of nanowires on the surface may stem from the longer second anodization time which would increase the exposure to the anodizing electrolytes, dissolving more of the nanowire residue. Exposure to the electrolytes used for detachment (1:1 ratio of ethanol and 78% perchloric acid) may have also contributed to the dissolution of the nanowire residue.

4.2.2 Cold Temperature Anodization

Figure 21a shows the surface of an alumina template that had undergone

anodization at 0 °C for the first anodization, etched at room temperature, re-anodized at 0

°C for 4 hours and detached at room temperature. Due to slower kinetics, a long second

anodization was needed to grow and detach a sturdy template. In Figure 21b, a higher

magnification image shows an average pore diameter of around 30 nm and 105 nm

average interpore distance.

(a)   (b)
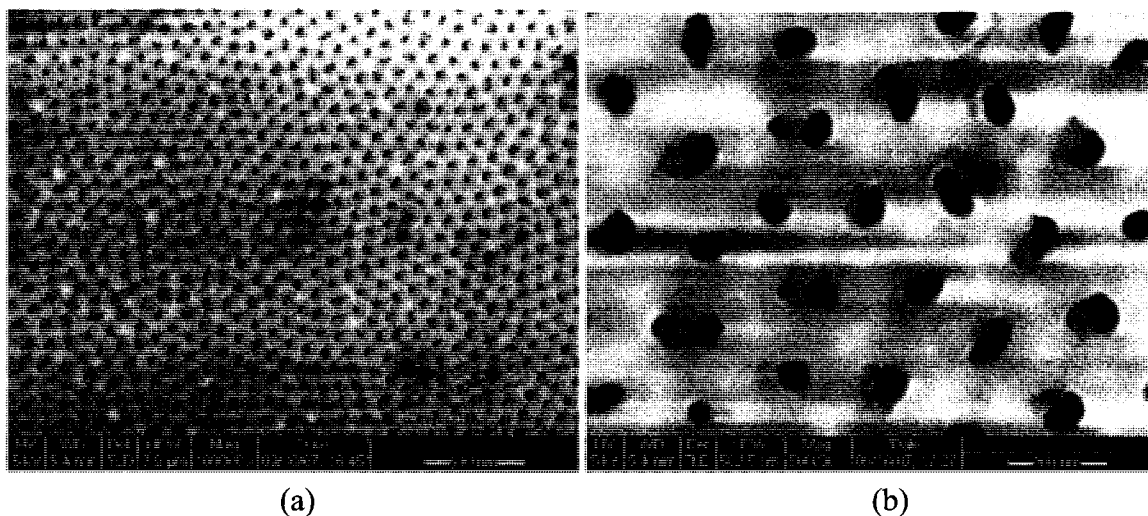
Figure 21. An SEM image of template after anodization at 0 °C at (a) 10000 X
and (b) 500000X.

Although the cold temperature anodization did not change the pore diameter or

interpore distance, the pores do appear different than the pores formed at room

temperature. The pores from the cold temperature anodization appear more asymmetric

than those made at room temperature. Furthermore, the hexagonal structure, while still

maintained, is not as pronounced and the surface appears smoother, lacking a descending

slope from the boundary between each pore cell to the pore itself as is present in the room

temperature anodized pores. The slower kinetics may explain the difference in the smoother pore surface, where slower dissolution rates due to the reduction in temperature allow the pores to grow more evenly. The less pronounced hexagonal structure may be from the result of incomplete self organization due to the slower kinetics from the first anodization, which was conducted for the same duration as the room temperature process. The surface did not contain the nanowires observed on the template derived from the room temperature anodization, probably because the growth rate of the alumina is slower. The resulting alumina layer after the first anodization would be thinner than the room temperature processed template, leaving less available material to etch through.

4.2.3   Crystallinity of Alumina Templates at Various Temperatures

In the course of preparing nanowires, a gel filled commercial template was annealed to 1000 °C. The template was found to have become chemically resistant to both acids and bases. To determine how temperature affected the template, commercial alumina templates were heat treated for 3 hours at 600 °C and 900 °C. The XRD spectra of the commercial templates as received and heat treated were taken. The samples as received and annealed at 600 °C only showed large broad peaks indicative of an amorphous material as shown in Figure 22.
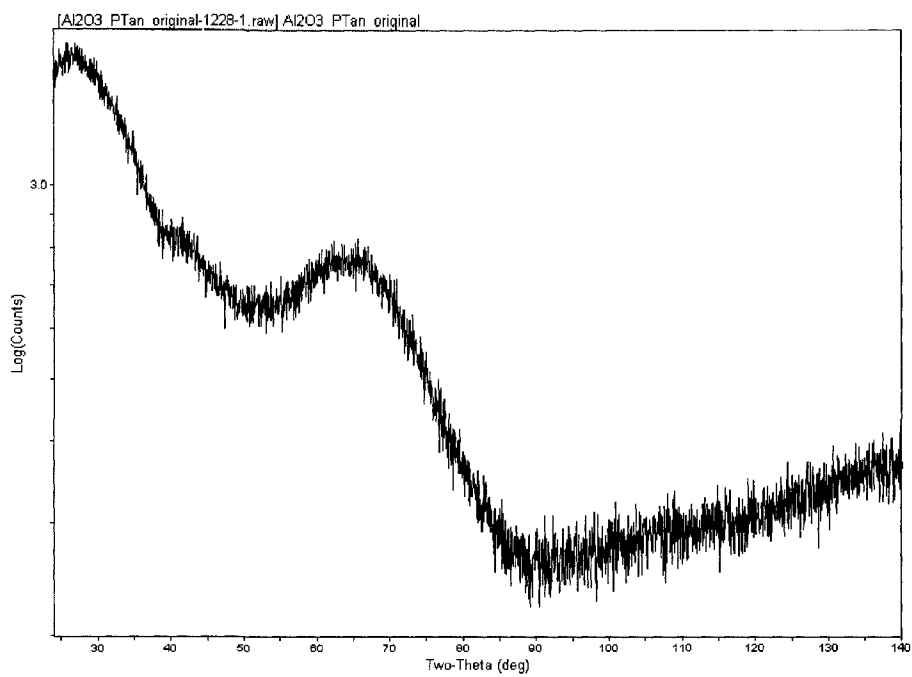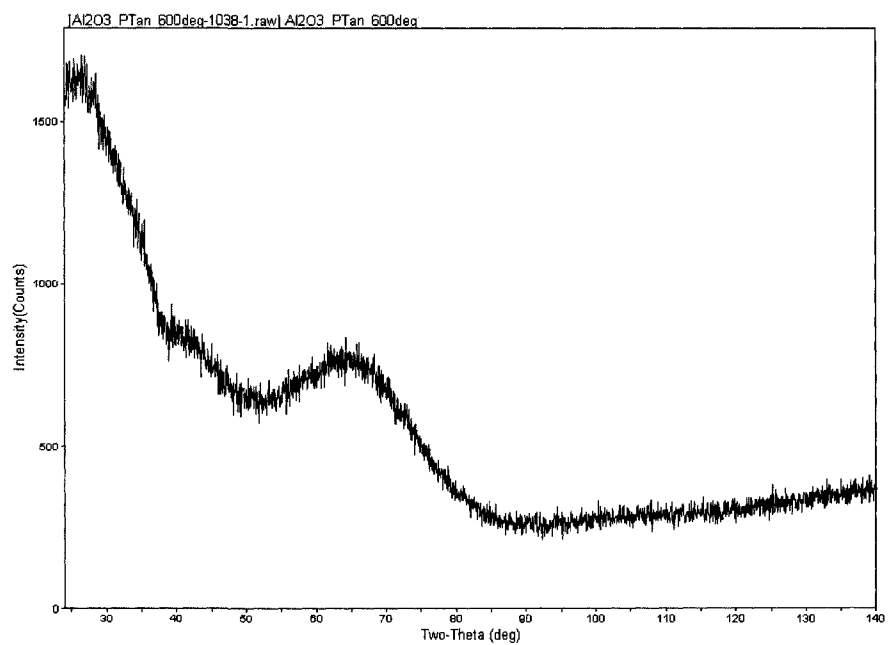
Figure 22.   An XRD spectrum of an alumina template annealed (a) as received and (b) annealed 3 hours at a temperature of 600 °C. The broad peaks indicate that the samples are amorphous.

58

The template annealed at 900 °C however, showed a number of sharp peaks indicative of a crystalline material. Analysis of the diffractogram show that the closest matching phase is that of γ-alumina, shown in Figure 23. This result indicates that templates should not be annealed to 900 °C if the dissolution of the template is required. More experiments should be done to determine the lower limit of the template's annealing temperature.
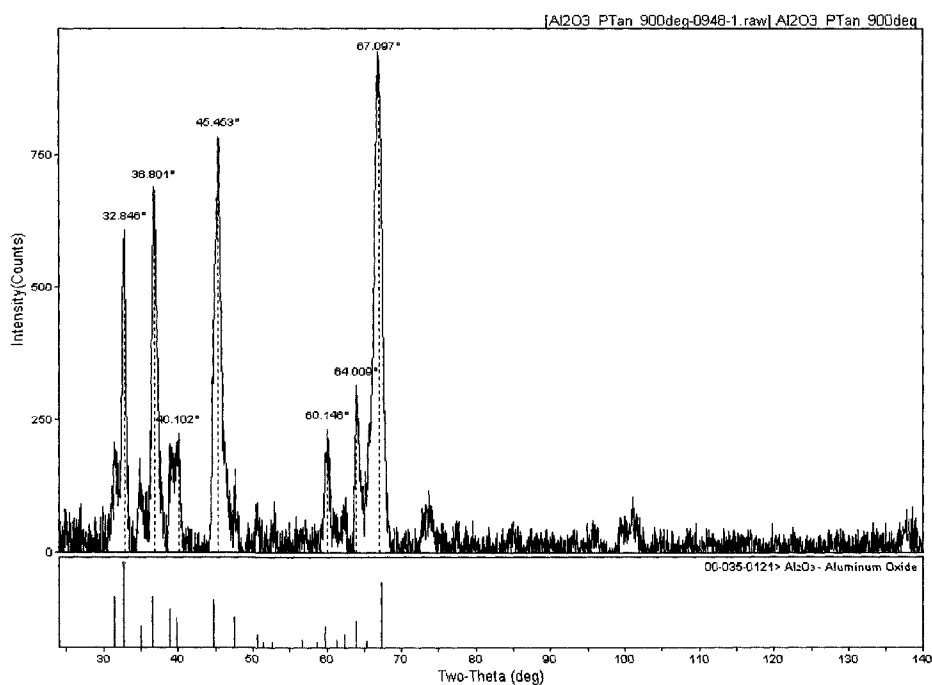
Figure 23.   An XRD spectrum of an alumina template annealed for 3 hours at a temperature of 900 °C.

4.3   Nickel Oxide Nanowires

Nickel oxide nanowires were synthesized using both fabricated template as well as a commercial template. Section 4.3.1 discusses the morphology of the resulting

nanowires. Section 4.3.2 discusses the composition of the nanowires, and Section 4.3.3

discusses the structure of the nanowires.

4.3.1   Morphology

NiO nanowires were successfully synthesized using a fabricated template with

pore diameters of around 50 nm as well as a commercial template with pore diameter of

200 nm. Figure 24 shows the image of the fabricated template actually used for the

synthesis.
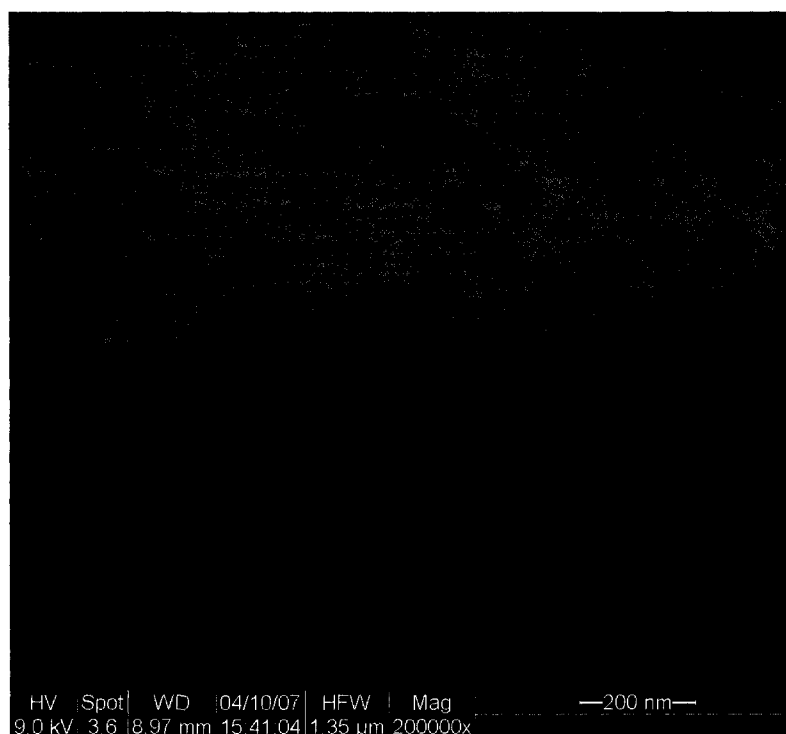
Figure 24. An SEM image of the alumina template used to synthesize NiO
nanowires.

Because of the smaller size of the NiO nanowires synthesized using the fabricated template, as well as their low conductivity, the nanowires were sputtered with 10 nm of gold to improve imaging. Figure 25 shows an SEM image of the NiO nanowire synthesized using the fabricated template. The diameter of the nanowire as it appears in the image is approximately 50 nm, however, this includes the layer of gold. The nanowire is thinner than the template probably due to contraction of the material in the annealing phase.
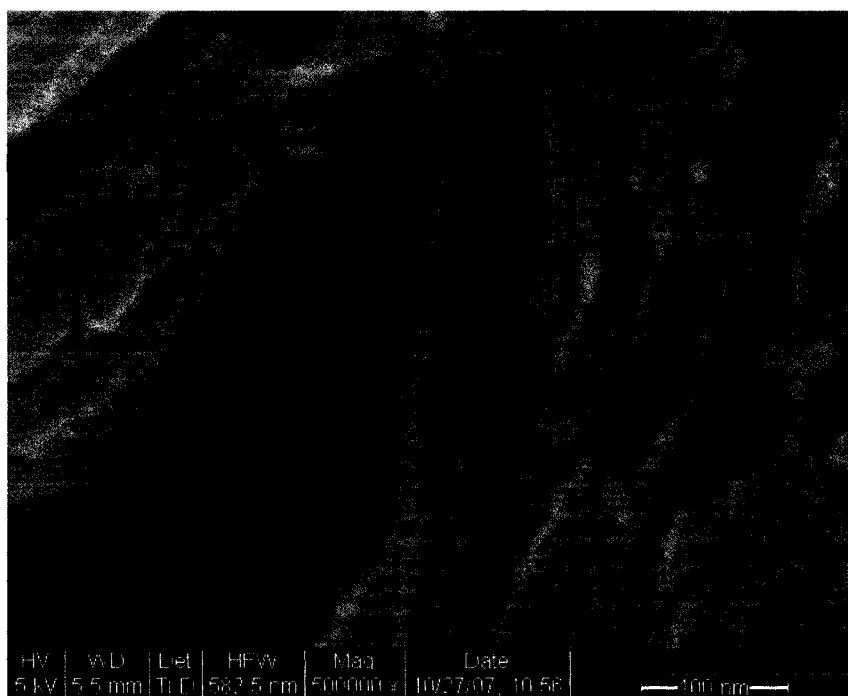
Figure 25. An SEM micrograph of gold sputtered NiO nanowires on a partially dissolved alumina template with pore diameters of approximately 50 nm.

An image of NiO nanowire synthesized using a commercial template is shown in Figure 26. This nanowire was not gold sputtered and the texture of the nanowire surface can be observed. The diameter of the nanowire is approximately 150 nm. Again,

contraction led to nanowire diameters smaller than the template pore diameters. The

surface appears to be rough and suggests that the nanowire may be composed of smaller

crystallites of NiO.

The nanowire's observed diameter matches the template pore size for both

commercial and fabricated templates. The technique of using pore size controlled

templates to control nanowire diameters appear to work.
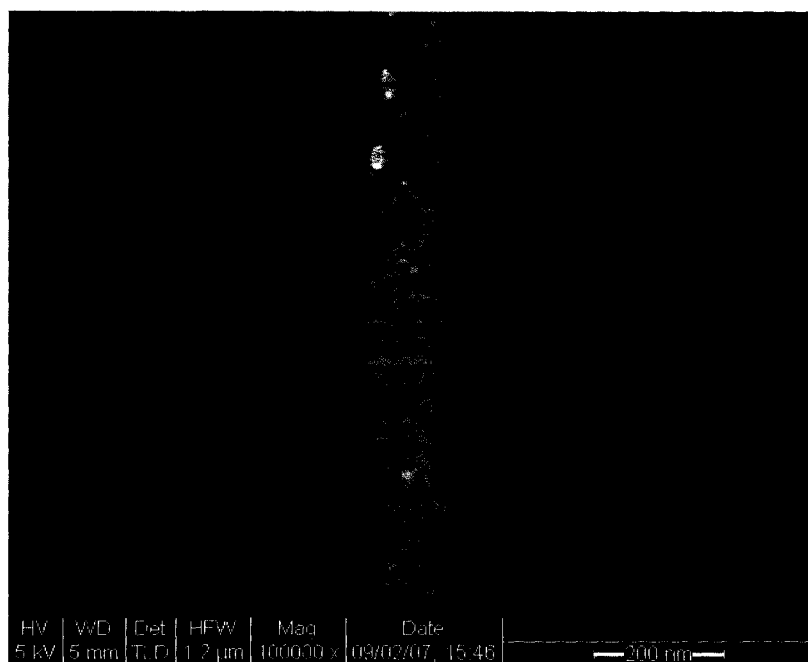
Figure 26.   An SEM image of a NiO nanowire synthesized from a commercial
alumina template.

4.3.2   Composition

The elemental analyses of the NiO nanowires are shown in Figures 27a and 27b.

Figure 27a shows the elemental analysis of the nanowires using the fabricated template.

The Ni and O peaks are clearly visible. The oxygen peak has contributions from both the

alumina (Al_2O_3) template and the NiO. The Na peak derives from the NaOH used to

partially dissolve the template and the Al comes from the alumina template. The small Si

and C peaks are from the SiC paper used to sand off the top layer of NiO on the template.

Since the template was very fragile, it was rinsed very gently with deionized water, but

this may not have removed the silicon carbide residue from the sandpaper. Figure 27b is

the elemental analysis of the NiO nanowires on the commercial template. The analysis of

the peaks is similar to that of Figure 27a except that the Si and C peaks are not present.

The sturdier template allowed a more thorough rinsing which probably removed the SiC

residue from the sandpaper.

The data shows that the nanowires contain the expected elements Ni and O,

although the contribution to the oxygen peak from alumina obscures the stoichiometry.

The XRD data discussed in the next section gave more conclusive results.

(a)
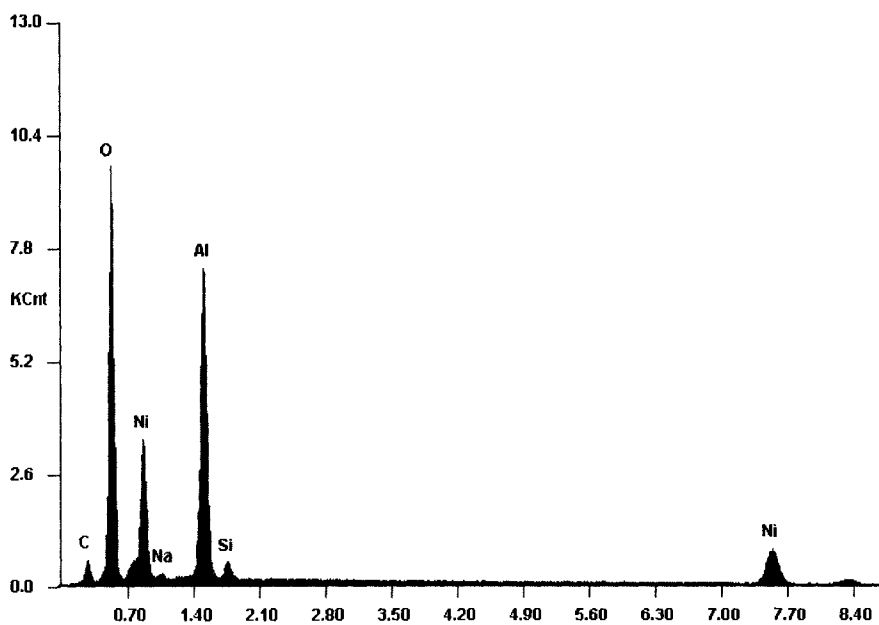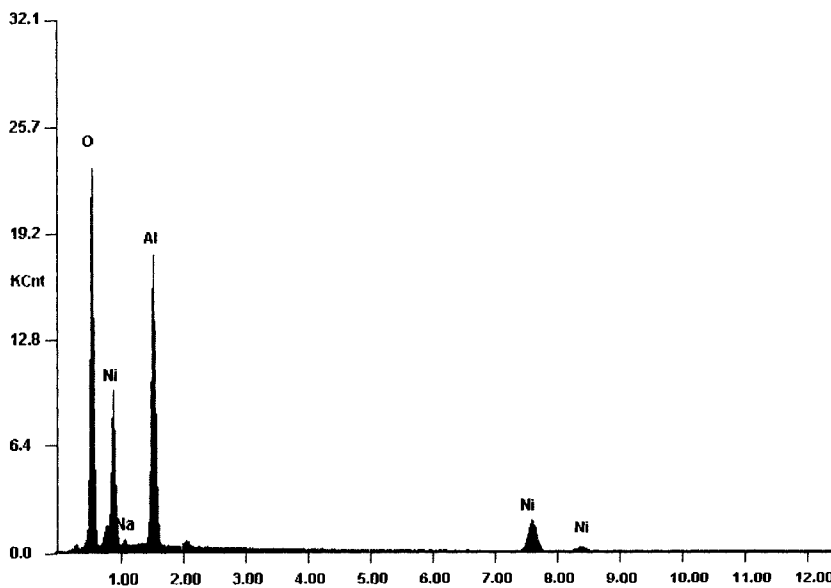
(b)

Figure 27. Elemental analysis results for NiO nanowires attached to a partially dissolved (a) fabricated alumina template and (b) commercial template.

4.3.3 Structure

To determine the crystal structure of the nanowires, a sample synthesized using commercial templates were sent to Rigaku Americas Corporation in Texas for XRD analysis, which is shown in Figure 28.
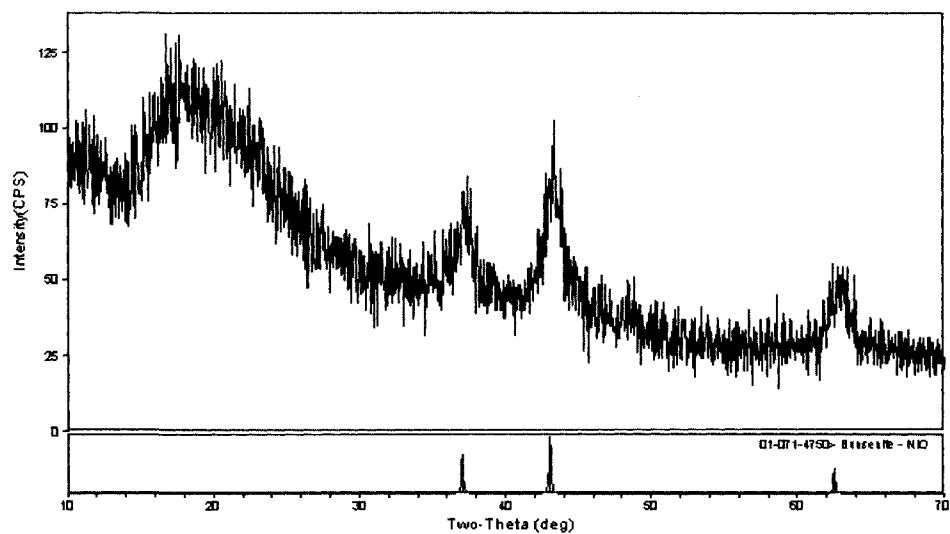
Figure 28. A graph of the XRD spectrum obtained from Rigaku.

The peak placement and intensity show that the analyzed material is a polycrystalline bunsenite, which is nickel (II) oxide with a cubic crystal structure. A large amorphous peak is visible from 10 to 30 degrees, probably from the alumina template. The results agree with findings in the literature. Analysis of the nanowires synthesized using the fabricated template was precluded due to the scarcity of the sample as well as the fragility of the template.

4.4   Hematite Nanowires

Hematite (α-Fe$_2$O$_3$) nanowires were synthesized using commercial templates with

200 nm pore diameter. An SEM image of a nanowire is shown in Figure 29.
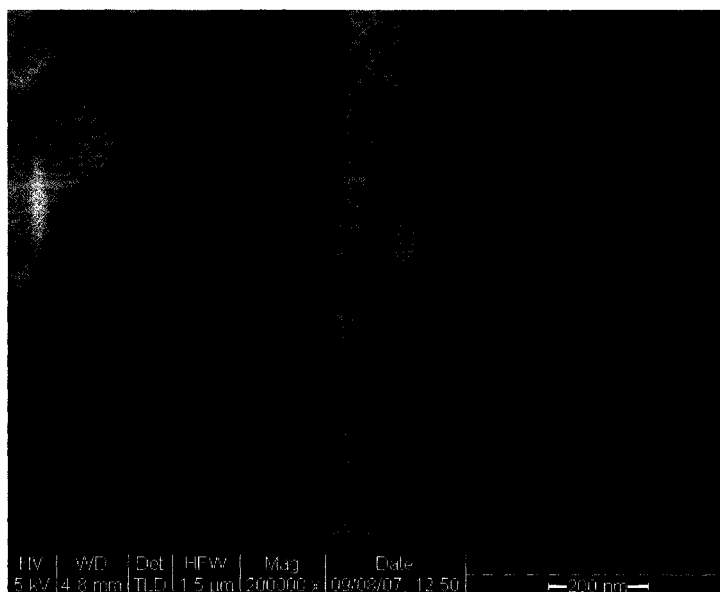
Figure 29. An SEM image of a hematite nanowire.

The diameter of the nanowire is approximately 200 nm. The texture of the

nanowire surface is uneven. Figure 30 shows an XRD diffractogram of the α-Fe$_2$O$_3$

nanowires still attached to the template. The peak placement and intensities indicate that

the sample is polycrystalline hematite, which is a hexagonally structured form of iron

oxide.

[Fe2O3-1619-6.raw] Fe2O3 - Full Chart

Hematite - synthetic - Fe2O3   33.190°/100.0%

PDF#97-002-2505: QM=Calculated; d=Calculated; I=(Unknown)
Hematite - synthetic
Fe2O3

2-Theta	d(Å)	I(f)	(h k l)	Theta	1/(2d)	2pi/d	n2
24.153	3.6817	30.1	(0 1 2)	12.077	0.1358	1.7066	
33.164	2.6992	100.0	(1 0 4)	16.582	0.1852	2.3278	
35.640	2.5171	71.4	(1 1 0)	17.820	0.1986	2.4962	
39.287	2.2914	1.7	(0 0 6)	19.644	0.2182	2.7421	
40.870	2.2082	22.4	(1 1 3)	20.435	0.2266	2.8479	
43.519	2.0779	1.9	(2 0 2)	21.759	0.2406	3.0238	
49.473	1.8409	39.1	(0 2 4)	24.736	0.2716	3.4132	
54.078	1.6944	47.3	(1 1 6)	27.039	0.2951	3.7081	

35.625°/48.6%
29.872°/28.3%
34.993°/26.8%
24.177°/23.0%
40.905°/21.9%
49.466°/20.4%
54.068°/36.7%

97-002-2505> Hematite - Fe2O3

Two-Theta (deg)

SAN JOSE STATE UNIV   [SANJOSE-ULTIMA0|Administrator]<C:\Windmax\Data\20070719> Friday, July 20, 2007 01:53p (MDI/JADE9)

Figure 30. An XRD spectrum of hematite nanowires embedded in alumina template.

4.5   Silicon Carbide Nanowires

In attempting to synthesize silicon carbide using the method by Hasegawa et al. [60], it was found that the alumina template becomes resistant to chemical attack after the annealing stage at 1000 °C. Section 4.5.1 discusses an alternative annealing procedure that was attempted to work around the problem presented by the template, and Section 4.5.2 discusses the compositional and structural analysis of the bulk material produced by the following the procedures based on Hasegawa et al. [60] and Gundiah et al. [67].

4.5.1   Alternative Annealing Process

Since the silicon carbide samples required annealing at 1000 °C and above, the

67

template could not be used because it would crystallize and become chemically resistant to etching. A different method to grow and extract the nanowires had to be explored.

First, to determine if the sol had penetrated the template pores during the dipping stage, the template was left to air dry for a few hours after dipping and then partially dissolved with 6 M NaOH. Figure 31 shows the partially dissolved template where the gel had infiltrated the pores and acquired a nanowire morphology.

Figure 31. An SEM image of the dried nanowire gel attached to a partially dissolved alumina template.

Since the gel was able to infiltrate the pores, a partial annealing experiment was attempted. A template dipped into the sol was left to dry for a few hours and then annealed at 600 °C. The template was then partially dissolved and an SEM image of this sample was taken as shown in Figure 32.
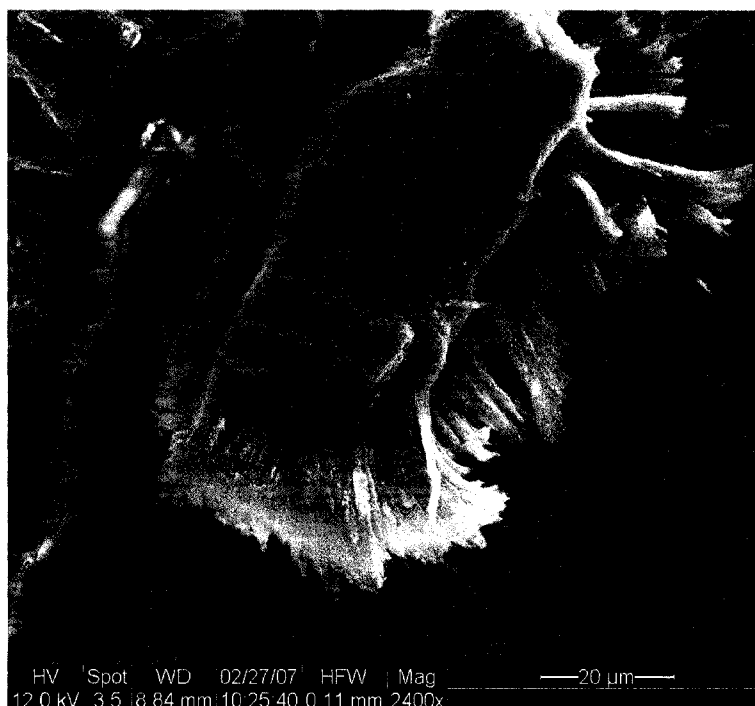
Figure 32. An SEM image of the template infiltrated with gel, partially dissolved then annealed to an intermediate temperature of 600 °C.

The sample image shows that the dehydrated gel, also known as xerogel, generally maintained the fibrous morphology of nanowires. However, they appear more rigid than that of the un-annealed sample. An EDS spectrum was taken to determine the elemental composition of the material, shown in Figure 33. The spectrum shows a strong C, Si and O peak as well as small Na peaks from the NaOH as well as some Al from the template.
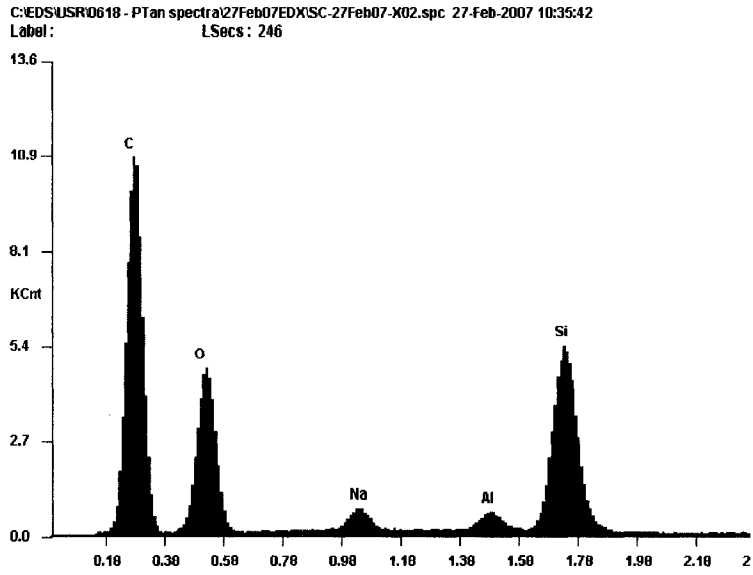
Figure 33. EDS results for the template infiltrated with gel, partially dissolved then annealed to an intermediate temperature of 600 °C.

To conclude the experiment, a partially dissolved pre-baked sample was annealed at 1000 °C and observed by SEM as shown in Figure 34. The image shows that the wires have started to congeal; the ends attached to the template still appear somewhat fibrous, but the further away from the template, the more congealed the material becomes.

Figure 34. An SEM image of the template infiltrated with gel, partially dissolved then annealed to 600 °C and then again at 1000 °C.

70

In addition to the unfortunate congealing of the nanowires, the elemental analysis

of the sample presented in Figure 35 also showed that the C peak has disappeared. A

likely explanation for the disappearance of the C peak is from reaction with stray oxygen

to form CO or CO_2.

C:\EDS\USR\0618 - PTan spectra\06Mar07EDX\SC-06Mar07-1.spc 06-Mar-2007 16:04:21
Label: LSecs: 75
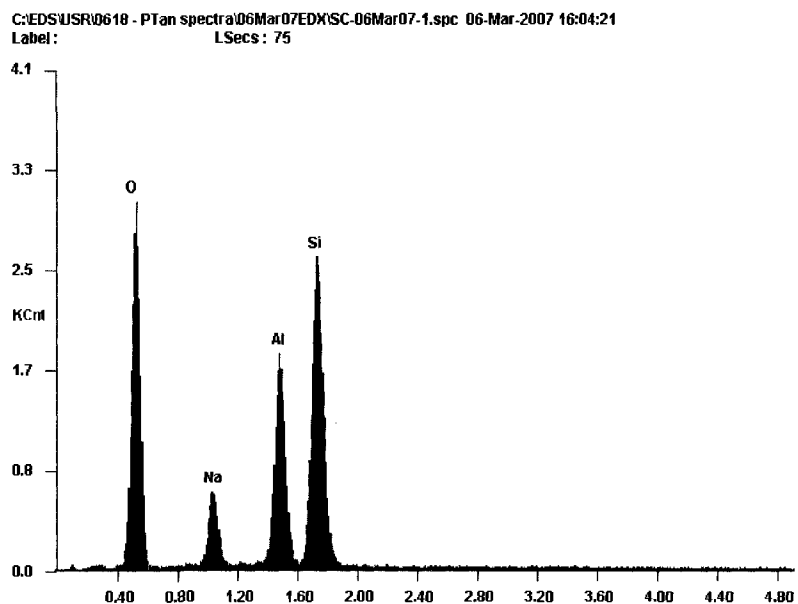
Figure 35. EDS results for the template infiltrated with gel, partially dissolved
then annealed to 600 °C and then again at 1000 °C.

4.5.2 Structure

To determine if any SiC at all was produced, bulk gel was subjected to the 1000

°C annealing process. Both procedures from Hasegawa *et al.* [60] as well as Gundiah *et*

al. [67] did not yield any XRD peaks, indicating that the gel was still amorphous and

crystalline SiC was not produced as shown in Figure 36.
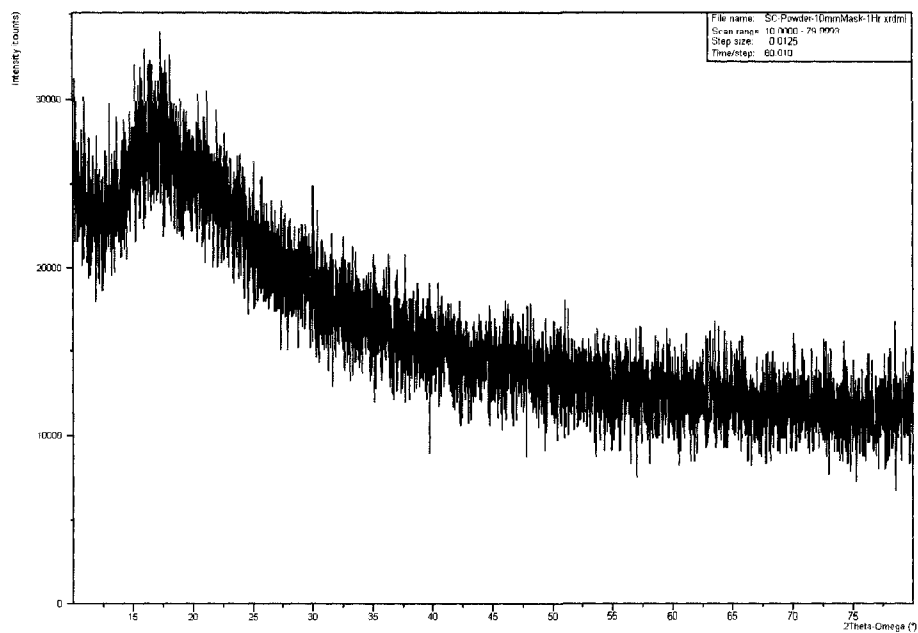
(a)
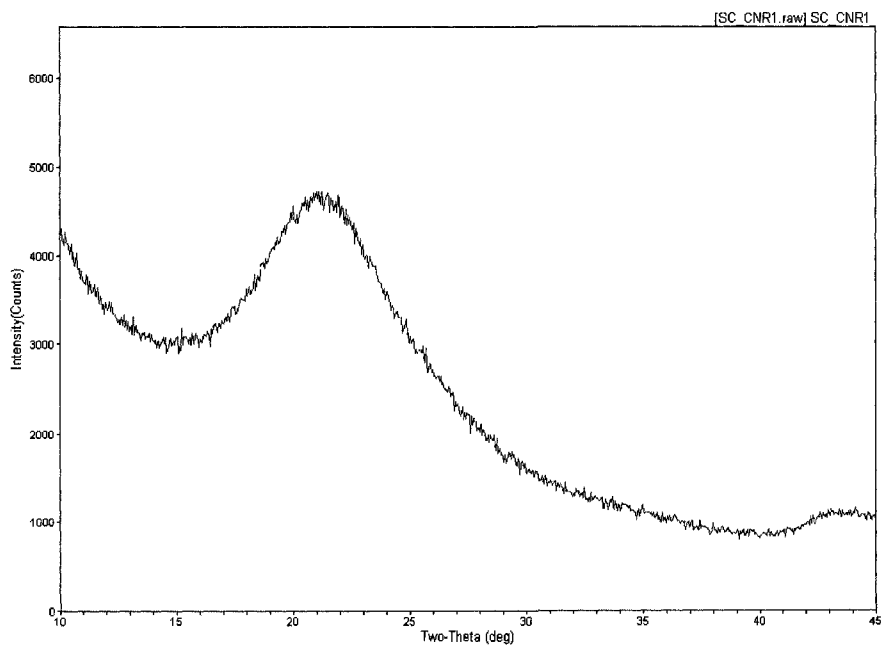
(b)

Figure 36. An XRD scan of annealed bulk gel obtained from a modified procedure by (a) Hasegawa *et al.* [60] and (b) Gundiah *et al.* [76].

CHAPTER FIVE

SUMMARY AND CONCLUSIONS

5.1   Summary

Alumina templates were synthesized using room temperature and cold temperature anodization. The images from the template fabricated at room temperature showed that uneven pores and non-hexagonal pore arrangements developed at the surface during the first anodization. However, uniform pores and a hexagonally ordered pore arrangement developed at the aluminum/alumina boundary as evidenced by the pore imprint found on the aluminum after etching. The second anodization at room temperature produced ordered hexagonal pore arrangements with pore diameters of around 50 nm and interpore distances of 115 nm. The etching phase did not completely strip the alumina layer produced from the first anodization but left what appeared to be nanowires on the surface. These nanowires may have been the result of a combination of uneven etching due to the double-layered structure of the pore as well as the differences in thickness at the points and edges of the hexagonally oriented pore structures. The second anodization process removed some of the nanowires from the surface. A longer duration for the second anodization coupled with a detachment phase also appeared to decrease the volume of nanowires on the surface. The presence of the alumina nanowires indicate that a better etching process is needed, but may also present an intriguing method of creating alumina nanowires.

The pore features for the template following the 0 °C anodization procedure were similar to that of the template made using the room temperature anodization procedure, with pore diameter of about 30 nm and interpore distances of about 105 nm. The appearance of the pores for this procedure is somewhat different from the template made using the room temperature anodization procedure: the pores are more asymmetric yet the surface appears smoother.

Crystallization of the amorphous commercial alumina templates does not occur at temperatures below 600 °C. At 900 °C, crystallization occurs, resulting in γ-phase alumina.

NiO and α-Fe$_2$O$_3$ nanowires were successfully synthesized. The NiO nanowires were made from a fabricated template and a commercial template while the α-Fe$_2$O$_3$ was made with only a commercial template. The diameters of the nanowires were in accordance with the template pore diameter though somewhat thinner due to contraction during the annealing phase. Silicon carbide nanowires could not be synthesized using the techniques attempted here.

5.2   Suggestions for Future Work

The presence of nanowires on the surface of the alumina templates was unexpected. Further investigation and a procedure to crystallize and extract these nanowires would be worthwhile. A suggestion for this work is to attempt the detachment procedure on the substrate after the etching phase and crystallize the nanowires at 900 °C.

Alternatively, nanowires may be detached through sonication and concentrated using centrifugation. The precipitate can then be spread on a silicon substrate and annealed at 900 °C for crystallization.

To improve the etching portion of the anodization process, stronger etchants such as 1 M sodium hydroxide or a chromic-phosphoric acid mixture as detailed by Shingubara [71] should be explored.

The difficulty of obtaining SiC nanowires is due to the annealing temperature being too low and the crystallization of the alumina template, which cannot be removed after the annealing phase. A few suggestions to overcome some of these issues in future experiments are included here.

SiC synthesis using high temperatures (≥ 1200 °C) should be attempted. An alternative may be to decrease the pressure of the system to enhance the vaporization of SiO_2 which then reduces to SiO, a key reagent in the carbothermal reduction process.

Since the sol-gel carbothermal reduction process has been shown to produce nanowires, a study on the effect of varying processing conditions such as annealing temperature, time and operating pressure on the nanowire growth may provide insight as to how to control SiC nanowire dimensions without a template.

REFERENCES

1. Feynman, R.P. (1959). *Feynman's talk*. http://www.zyvex.com/nanotech/feynman.html (accessed 26 September 2006). WWW Article.

2. T. Sargent, The Dance of Molecules. How Nanotechnology is Changing Our Lives. (Thunder's Mouth Press. New York, NY 2006), pp. 7-22.

3. S. Iijima, "*Helical microtubules of graphitic carbon*," Nature, **345**, pp. 56-58 (1991).

4. M.F. Yu, O. Lourie, M.J. Dyer, K. Moloni, T.F. Kelly and R.S. Ruoff, "*Strength and breaking mechanism of multiwalled carbon nanotubes under tensile load*," Science, **287**, pp. 637-640 (2000).

5. M.S. Dresselhaus, G. Dresselhaus, and A. Jorio, "*Unusual properties and structure of carbon nanotubes*," Annu. Rev. Mater. Res., **34**, pp. 247-278 (2004).

6. Y. Cui, Z. Zhong, D. Wang, W.U. Wang and C.M. Lieber, "*High performance silicon nanowire field effect transistors*," Nano Lett., **3(2)**, pp. 149-152 (2003).

7. E. Tutuc, J. Appenzeller, M.C. Reuter and S. Guha, "*Realization of a linear germanium nanowire p-n junction,* " Nano Lett., **6(9)**, pp. 2070-2074 (2006).

8. Y. Huang, X. Duan, T. Cui, L.J. Lauhon, K.H. Kim and C.M. Lieber, "*Logic gates and computation from assembled nanowire building blocks,*" Science, **294(5545)**, pp. 1313-1317 (2001).

9. N. Amin and S. Arajs, "*Morin temperature of annealed submicronic α-Fe_2O_3 particles,*" Phys. Rev. B, **35**(10), pp. 4810-4811 (1987).

10. G.F. Zhang, F. Patolsky, Y. Cui, W.U. Wang and C.M. Lieber, "*Multiplexed electrical detection of cancer markers with nanowire sensor arrays,*" Nature Biotechnol., **23**, pp. 1294-1301 (2005).

11. Y. Li, F. Qiana, J. Xianga and C.M. Lieber, "*Nanowire electronic and optoelectronic devices,*" Materials Today, **9**, pp. 18-27 (2006).

12. W. Yang, H. Araki, A. Kohyama, Q. Yang, Y. Xu, J. Yu and T. Noda, "*The effect of SiC nanowires on the flexural properties of CVI-SiC/SiC composites,*" J. Nucl. Mater., **367-370(1)**, pp. 708-712 (2007).

13. Z.L. Wang, Z. Zhang and Y. Liu, Handbook of Nanophase and Nanostructured Materials. (Klewer Academic/Plenum Publishers. New York, NY 2003), pp. 151-153.

14. T. Stelzner, G. Andra, F. Falk, E. Wendler, E. Wesch. R. Scholz and S. Christiansen, *"Silicon nanowire synthesis on metal implanted silicon substrates,"* Nucl. Instrum. Meth. B, **257**, pp. 172-176 (2007).

15. X.M. Cai, A.B. Djurisic and M.H. Xie, *"GaN nanowires: CVD synthesis and properties,"* Thin Solid Films, **515**, pp. 984-989 (2006).

16. D.M. Qu, P.X. Yan, J.B. Chang, D. Yan, J.Z. Yue, R.F. Zhuo and H.T. Feng, *"Nanowires and nanowire-nanosheet junctions of SnO2 nanostructures,"* Mater. Lett., **61**, pp. 2255-2258 (2007).

17. K. Woo, H.J. Lee, J.P. Ahn and Y.S. Park, *"Sol-gel mediated synthesis of Fe_2O_3 Nanorods,"* Adv. Mater., **15(20)**, pp. 1761-1764 (2003).

18. J. Liu, J.L. Duan, M.E. Toimil-Molares, S. Karim, T.W. Cornelius, D. Dobrev, H.J. Yao, Y.M. Sun, M.D. Hou, D. Mo, Z.G. Wang and R. Neumann, *"Electrochemical fabrication of single-crystalline and polycrystalline Au nanowires: the influence of deposition parameters,"* Nanotechnol., **17(8)**, pp. 1922-6 (2006).

19. H. Pan, B. Liu, J. Yi, C. Poh, S. Lim, J. Ding, Y. Feng, C.H.A. Huan and J. Lin, *"Growth of single-crystalline Ni and Co nanowires via electrochemical deposition and their magnetic properties,"* J. Phys. Chem. B, **109(8)**, pp. 3094-3098 (2005).

20. L. Sun and P.C. Searson, *"Electrochemical deposition of nickel nanowire arrays in single-crystal mica films,"* Appl. Phys. Lett., **74(19)**, pp. 2803-2805 (1999).

21. A.W. Zhao, C.H. Ye, G.W. Meng, L.D. Zhang and P.M. Ajayan, *"Tellurium nanowire arrays synthesized by electrochemical and electrophoretic deposition,"* J. Mater. Res., **18(10)**, pp. 2318-2322 (2003).

22. Y. Lin, F.Q. Sun, X.Y. Yuan, B.Y. Geng and L.D. Zhang, *"Sol-gel electrophoretic deposition and optical properties of Fe_2O_3 nanowire arrays,"* Appl. Phys. A, **78**, pp. 1197-1199 (2004).

23. Y.C. Wand, I.C. Leu and M.H. Hon, *"Dielectric property and structure of anodic alumina template and their effects on the electrophoretic deposition characteristics of ZnO nanowire arrays,"* J. Appl. Phys., **95(3)**, pp. 1444-1448 (2004).

24. B. Wang, Y. Shi and D. Xue, "Large aspect ratio titanate nanowire prepared by monodispersed titania submicron sphere via simple wet-chemical reactions," J. Solid State Chem., **180(3)**, pp. 1028-1037 (2007).

25. C.K. Xu, K.Q. Hong, S. Liu, G.H. Wang and X.M. Zhao, "*A novel wet chemical route to NiO nanowires,*" J. Cryst. Growth, **255**, pp. 308-312 (2003).

26. L. Wu, Y.S. Wu, H.Y. Wei, Y.C. Shi and C.X. Hu, "*Synthesis and characterization of NiO nanowires by a solution method,*" Mater. Lett., **58**, pp. 2700-2703 (2004).

27. G.Q. Jin, P. Liang and X.Y. Guo, "*Novel method for synthesis of silicon carbide nanowires,*" J. Mater. Sci. Lett., **22**, pp. 767-770 (2003).

28. Q. Yang, J. Sha, X.Y. Ma and D. Yang, "*Synthesis of NiO nanowires by a sol-gel process,*" Mater. Lett., **59**, pp. 1967-1970 (2005).

29. P.C. Hiemenz and R. Rajagopalan, Principles of Colloid and Surface Chemistry 3rd edition. (Marcel Dekker, Inc. New York, NY, 1997), pp. 1-37.

30. J.C. Brinker, Sol-Gel Science: The Physics and Chemistry of Sol-Gel Processing. (Academic Press. Boston, MA, 1990), pp. 36-78.

31. M.E. Toimil Morales, J. Brotz, V. Buschmann, D. Dobrev, R. Neumann, R. Scholz, I.U. Schuchaert, C. Trautmann and J. Vetter, "*Etched heavy ion tracks in polycarbnate as template for copper nanowires,*" Nucl. Instrum. Meth. B, **185**, pp. 192-197 (2001).

32. R.J. Tonucci, B.L. Justus, A.J. Campillo and C.E. Ford, "*Nanochannel array glass,*" Science, **258**, pp. 783-784 (1992).

33. L. Sun, C.L. Chien and P.C. Searson, "*Fabrication of nanoporous single crystal mica templates for electrochemical deposition of nanowire arrays,*" J. Mater. Sci., **35**, pp. 1097-1103 (2000).

34. W.H. Gitzen, Alumina as a Ceramic Material. (The American Ceramic Society, Westerville, 1970), p. 17

35. M. Yu, J. Liu and S. Li, "*Preparation and characterization of highly ordered NiO nanowire arrays by sol-gel template method,*" Journal of University of Science and Technology Beijing, Mineral, Metallurgy, Material, **13**, pp. 169-173 (2006).

36. H. Cao, X. Qio, Y. Liang, M. Zhao and Q. Zhu, "*Sol-gel template synthesis and photoluminescence of n- and p-type semiconductor oxide nanowires,*" ChemPhysChem, **7**, pp. 497-501 (2006).

37. L. Suber, P. Imperatori, G. Ausanio, F. Fabbri and H. Hofmeister, "*Synthesis, morphology, and magnetic characterization of iron oxide nanowires and nanotubes,*" J. Phys. Chem. B, **109**, pp. 7103-7109 (2005).

38. C. Wu, P. Yin, X. Zi, C.O. Yang and Y. Xie, "*Synthesis of hematite (α-Fe$_2$O$_3$) nanorods: diameter-size and shape effects on their applications in magnetisc, lithium ion battery and gas sensors,*" J. Phys. Chem. B, **110**, pp. 17806-17812 (2006).

39. A. Agarwal and S.E. Saddow, <u>Advances in Silicon Carbide Processing and Applications</u>. (Artech House, Inc. Norwood, MA, 2004), pp. 1-5.

40. G.E. Thompson, R.C. Furneaux, G.C. Wood, J.A. Richardson and J.S. Goode, "*Nucleation and growth of porous anodic films on aluminium,*" Nature, **272**, pp. 433-435 (1978).

41. G.E. Thompson and G.C. Wood, "*Porous anodic film formation on aluminium,*" Nature, **290**, pp. 230-232 (1981).

42. H. Masuda and K. Fukuda, "*Ordered metal nanohole arrays made by a two-step replication of honeycomb structures of anodic alumia,*" Science, **268**, pp. 1466-1468 (1995).

43. O. Jessensky, F. Muller and U. Gosele, "*Self-organized formation of hexagonal pore arrays in anodic alumina,*" Appl. Phys. Lett., **72(10)**, pp. 1173-11755 (1998).

44. K. Nielsch, J. Choi, K. Schwirn, R.B. Wehrspohn and U. Gosele, "*Self-ordering regimes of porous alumina: The 10% porosity rule,*" Nano Lett., **2(7)**, pp. 677-680 (2002).

45. F. Li, L. Zhang and R.M. Metzger "*On the growth of highly ordered pores in anodized aluminum oxide,*" Chem Mater., **10**, pp. 2470-2480 (1998).

46. D. Routkevitch, T. Bigioni, M. Moskovits and J.M. Xu, "*Electrochemical fabrication of CdS nanowire arrays in porous anodic aluminum oxide templates,*" J. Phys. Chem., **100(3)**, pp. 14037-14046 (1996).

47. S.J. Chu, K. Wada, S. Inoue and S. Todoroki, "*Fabrication and characterization of ordered Ni Nanostructures on glass by anodization and direct current electrodeposition*," Chem. Mater., **14**, pp. 4595-4602 (2002).

48. S.J. Chu, K. Wada, S. Inoue and S. Todoroki, "*Synthesis and characterization of titania nanostrictures on glass by Al anodization and sol-gel process*," Chem. Mater., **14**, pp. 266-272 (2002).

49. H. Masuda, M. Nagae, T. Morikawa and K. Nishio, "*Long-range-ordered anodic porous alumina with reduced hole interval formed at highly concentrated sulfuric acid solution*," Jpn. Soc. Appl. Phys., **45(14)**, pp. L06-L408 (2006).

50. S.Z. Chu, K.Wada, S. Inoue, M. Isogai, Y, Katsunta and A. Yasumori, "*Large-scale fabrication of ordered nanoporous alumina films with arbitrary pore intervals by critical-potential anodization*," J. Electrochem. Soc., **153(9)**, pp. B384-B391 (2006).

51. T. Dimogerontakis and I.Tsangaraki-Kaplanoglou, "*The role of aluminum anodizaing conditions on the effect of the additive light green*," Thin Solid Films, **402**, pp. 121-125 (2002).

52. S.Z. Chu, K.Wada, S. Inoue, M. Isogai, Y and A. Yasumori, "*Fabrication of ideally ordered nanoporous alumina films and integrated alumina nanotubule arrays by high-field anodization*," Adv. Mater., **17**, pp. 2115-2119 (2005).

53. T.T. Xu, R.D. Piner and R.S. Ruoff, "*An improved method to strip aluminum from porous anodic alumina films*," Langmuir, **19**, pp. 1443-1445 (2003).

54. J.H. Yuan, W. Chen, R.J. Hui and X.H. Xia, "*Mechanism of one-step voltage pulse detachment of porous anodic alumina membranes*," Electrochimica Acta, **51**, pp. 4589-4595 (2006).

55. W. Chen, J. Wu, J. Yuan, X. Xia and X. Lin, "*An environmentally-friendly electrochemical detachment method for porous anodic alumina*," J. Electroanal. Chem., **600**, pp. 257-264 (2007)

56. C.R. Martin, "*Nanomaterials: A membrane-based synthetic approach,*" Science, **266**, pp. 1961-1966 (1994).

57. F. Schlottig, M. Textor, U. Georgi and G. Roewer, "*Template synthesis of SiO₂ nanostructures*," J. Mater. Sci. Lett., **18**, pp. 599-601 (1999).

58. I.S. Seog and C.H. Kim, "*Preparation of monodispersed spherical silicon carbide by the sol-gel method*," J. Mater. Sci., **28**, pp. 3277-3282 (1993).

59. V. Raman, O.P. Bahl and U. Dhawan, "*Synthesis of silicon carbide through the sol-gel process from different precursors*," J. Mater. Sci., **30**, pp. 952-954 (2000).

60. I. Hasegawa, T. Nakamura, S. Motojima and M. Kajiwara, "*Silica gel-phenolic resin hybrid fibres: new precursors for continuous silicon carbide fibres,*" J. Mater. Chem., **5**, pp 193-194 (1995).

61. L. Cerovic, S.K. Milonjic and S.P. Zec, "*A comparison of sol-gel derived silicon carbide powders from saccharose and activated carbon,*" Ceram. Int., **21**, pp. 27 1-276 (1995).

62. V. Raman, V.K. Parashar and S. Dhakate, "*Synthesis of silicon carbide whiskers from substituted silicon alkoxides and rayon fibres,*" J. Sol-Gel Sci. Technol., **25**, pp. 175-179 (2002).

63. C.R. Rambo, J. Cao, O. Rusina and H. Sieber, "*Manufacturing of biomorphic (Si, Ti, Zr)-carbide ceramics by sol–gel processing,*" Carbon, **43**, pp. 1174-1183 (2005).

64. G.W. Meng, Z. Cui, L.D. Zhang and F. Phillipp, "*Growth and characterization of nanostructured β-SiC via carbothermal reduction of SiO_2 xerogels containing carbon nanoparticles,*" J. Cryst. Growth, **209**, pp. 801-806 (2000).

65. X.K. Li, L. Liu, Y.X. Zhang, S.D. Shen, S. Ge and L.C. Ling, "*Synthesis of nanometre silicon carbide whiskers from binary carbonaceous silica aerogels,*" Carbon, **39**, pp. 159-165 (2001).

66. C.H. Liang, G.W. Meng, L.D. Zhang, Y.C. Wu and Z. Cui, "*Large-scale synthesis of β-SiC nanowires by using mesoporous silica embedded with Fe nanoparticles,*" Chem. Phys. Lett., **329**, pp. 323-328 (2000).

67. G. Gundiah, G.V. Govindaraj, M.M. Seikh and C.N.R. Rao, "*Synthesis and characterization of silicon carbide, silicon oxynitride and silicon nitride nanowires,*" J. Mater. Chem., **12**, pp. 1606-1611 (2002).

68. B.S. Weakley, A Beginner's handbook in Biological Transmission Electron Microscopy, 2nd Edition. (Churchill Livingstone. New York, NY, 1981), pp. 1-17.

69. M. Postek, <u>Scanning Electron Microscopy a Student's Handbook.</u> (Ladd Research Industries, 1980), pp. 1-84.

70. A. Guinier, <u>X-Ray Diffraction in Crystals, Imperfect Crystals and Amorphous Bodies</u>. (W.H. Freeman and Co., San Francisco, CA, 1963), pp.1-.24, 94-118.

71. S. Shingubara, "*Fabrication of nanomaterials using porous alumina templates,*" J. Nanopart. Res., **5**, pp. 17-30 (2003).